Journal of Geophysical Research: Biogeosciences

RESEARCH ARTICLE
10.1029/2018JG004520

Large-Scale Droughts Responsible for Dramatic Reductions of Terrestrial Net Carbon Uptake Over North America in 2011 and 2012

Wei He[1,2], Weimin Ju[1,3], Christopher R. Schwalm[4,5], Sebastian Sippel[6], Xiaocui Wu[7], Qiaoning He[1,8], Lian Song[1], Chunhua Zhang[9], Jing Li[1], Stephen Sitch[10], Nicolas Viovy[11], Pierre Friedlingstein[10], and Atul K. Jain[12]

[1]International Institute for Earth System Science, Nanjing University, Nanjing, China, [2]Center for Isotope Research (CIO), Energy and Sustainability Research Institute Groningen, University of Groningen, Groningen, Netherlands, [3]Jiangsu Center for Collaborative Innovation in Geographic Information Resource Development and Application, Nanjing, China, [4]Woods Hole Research Center, Falmouth, MA, USA, [5]Center for Ecosystem Science and Society, Northern Arizona University, Flagstaff, AZ, USA, [6]Norwegian Institute of Bioeconomy Research, Ås, Norway, [7]Department of Microbiology and Plant Biology, Center for Spatial Analysis, University of Oklahoma, Norman, OK, USA, [8]School of Urban and Environmental Sciences, Huaiyin Normal University, Huaian, China, [9]School of Resources and Environmental Engineering, Ludong University, Yantai, China, [10]College of Life and Environmental Sciences, University of Exeter, Exeter, UK, [11]Laboratoire des Sciences du Climat et de l'Environnement, CEA CNRS UVSQ, Gif-sur-Yvette, France, [12]Department of Atmospheric Sciences, University of Illinois at Urbana-Champaign, Urbana, IL, USA

Key Points:
- Large NEP reductions in 2011 and 2012 are due to contrasting effects of GPP and Reco in the context of droughts
- Two temperate ecoregions crops/agriculture and grass/shrubs contributed largest to these reductions
- Compensation of drought-induced carbon uptake reductions due to warm spring occurred only in some specific ecoregions

Supporting Information:
- Figure S1

Correspondence to:
W. Ju,
juweimin@nju.edu.cn

Citation:
He, W., Ju, W., Schwalm, C. R., Sippel, S., Wu, X., He, Q., et al. (2018). Large-scale droughts responsible for dramatic reductions of terrestrial net carbon uptake over North America in 2011 and 2012. *Journal of Geophysical Research: Biogeosciences*, *123*, 2053–2071. https://doi.org/10.1029/2018JG004520

Received 30 MAR 2018
Accepted 5 JUN 2018
Accepted article online 14 JUN 2018
Published online 7 JUL 2018

Abstract Recently, severe droughts that occurred in North America are likely to have impacted its terrestrial carbon sink. However, process-based understanding of how meteorological conditions prior to the onset of drought, for instance warm or cold springs, affect drought-induced carbon cycle effects remains scarce. Here we assess and compare the response of terrestrial carbon fluxes to summer droughts in 2011 and 2012 characterized by contrasting spring conditions. The analysis is based on a comprehensive ensemble of carbon cycle models, including FLUXCOM, TRENDY v5, SiBCASA, CarbonTracker Europe, and CarbonTracker, and emerging Earth observations. In 2011, large reductions of net ecosystem production (NEP; −0.24 ± 0.17 Pg C/year) are due to decreased gross primary production (−0.17 ± 0.18 Pg C/year) and slightly increased ecosystem respiration (+0.07 ± 0.17 Pg C/year). Conversely, in 2012, NEP reductions (−0.17 ± 0.25 Pg C/year) are attributed to a larger increase of ecosystem respiration (+0.48 ± 0.27 Pg C/year) than gross primary production (+0.31 ± 0.29 Pg C/year), induced predominantly by an extra warmer spring prior to summer drought. Two temperate ecoregions crops/agriculture and the grass/shrubs contribute largest to these reductions and also dominate the interannual variations of NEP during 2007–2014. Moreover, the warming spring compensated largely the negative carbon anomaly due to summer drought, consistent with earlier studies; however, the compensation occurred only in some specific ecoregions. Overall, our analysis offers a refined view on recent carbon cycle variability and extremes in North America. It corroborates earlier results but also highlights differences with respect to ecoregion-specific carbon cycle responses to drought and heat.

1. Introduction

Terrestrial ecosystems offset approximately one fourth of global anthropogenic CO_2 emissions (Le Quéré et al., 2016), substantially slowing down the increase of CO_2 concentration in the atmosphere and the pace of global warming. However, climate extremes (e.g., droughts and extremely low or high temperature) exert strong impacts on carbon sequestration by terrestrial ecosystems (van der Molen et al., 2011). Understanding the effects of climate extremes on the terrestrial carbon cycle is paramount for studies on global climate change as well as natural resource and food security.

In recent decades, large-scale droughts have impacted many regions around the world (Ciais et al., 2005; Gatti et al., 2014; Zhao & Running, 2010), including North America (Luo et al., 2017; Schwalm et al., 2012; Wolf et al., 2016). For example, the 2012 summer drought over the Central Great Plains in the United States was reported as "the most severe seasonal drought in 117 years resulted mostly from natural variations in weather" (Hoerling et al., 2014). While many studies have examined the effects of droughts on the terrestrial carbon cycle, these typically focus on site or local scales (Biederman et al., 2016; Doughty et al., 2015;

Scott et al., 2015; Wolf et al., 2013). Only a few studies have examined at large scales (Jung et al., 2017; Schwalm et al., 2012; Wolf et al., 2016; Zscheischler et al., 2014). There are large knowledge gaps regarding the impacts of large-scale droughts on terrestrial carbon cycle due to a couple of challenges as below.

One big challenge in studying the impacts of large-scale droughts on the terrestrial carbon cycle is how to accurately estimate carbon fluxes over large regions, which are not directly measurable. A common way is to simulate carbon fluxes using bottom-up terrestrial biosphere models (TBMs), including a new generation of modeling approaches with a richer representation of functional diversity (i.e., dynamic global vegetation models, DGVMs, e.g., ORCHIDEE) and traditional modeling approaches based on a small number of fixed plant functional types (e.g., the combined Simple Biosphere/Carnegie-Ames-Stanford Approach [SiBCASA]). Owing to uncertainties in model inputs and parameters as well as the failure of models to capture carbon cycling processes, intermodel differences in simulated carbon fluxes are large (Huntzinger et al., 2012; Restrepo-Coupe et al., 2017). Atmospheric inversion models (AIMs), complementing bottom-up biosphere modeling, optimize net regional and global biosphere carbon fluxes by adjusting prior estimates from TBMs to match high-precision atmospheric CO_2 measurements (Peters et al., 2007; Peylin et al., 2013; van der Laan-Luijkx et al., 2017). At finer scales, the eddy covariance technique monitors net ecosystem production (NEP), on which gross primary production (GPP) and ecosystem respiration (Reco) could be estimated using partitioning approaches (Lasslop et al., 2010; Reichstein et al., 2005). These in situ CO_2 flux measurements can be upscaled to regions or the globe using remote sensing data and machine learning (ML) algorithms (Jung et al., 2017). Integration of carbon fluxes estimated using different approaches is a practical way to constrain uncertainties in estimated carbon fluxes.

Another challenge is associated with uncertainties in large-scale drought monitoring and the complexity of drought impacts on carbon fluxes, including not only land-atmosphere interactions concurrently to extreme events (Sippel et al., 2016; Wolf et al., 2016) but also inducing memory effects (Schwalm et al., 2017). Recent rapid development of satellite Earth observations (EO) makes it possible to monitor soil moisture (SM), underground water storage, and vegetation physiological activity—all valuable observations for monitoring hydrological and vegetation processes during droughts and to understand the impacts on the terrestrial carbon cycle. A number of emerging spaceborne data have also been employed for this purpose, such as solar-induced chlorophyll fluorescence (SIF; Sun et al., 2015; S. Wang et al., 2016), satellite SM (Nicolai-Shaw et al., 2017; Velpuri et al., 2016), and terrestrial total water storage (TWS; Cao et al., 2015; Xie et al., 2016; Yang et al., 2014; Yi & Wen, 2016). The synergy of different types of EO data might more effectively characterize droughts and helps to attribute their impacts on the terrestrial carbon cycle.

In 2011 and 2012, two large-scale droughts hit North America (Sun et al., 2015). In both years, strong summer droughts took place but with contrasting unusually cold (2011) and warm (2012) spring conditions that preceded summer drought. These meteorological differences thus offer an opportunity for a comparative analysis of spring-summer carbon cycle dynamics, which we hypothesized might lead to different carbon cycle responses. A recent study by Wolf et al. (2016) investigated the compensation effect of the spring warming to the summer drought impact on terrestrial net carbon uptake in the United States in 2012. However, several uncertainties remain, mainly with respect to the impact of different meteorological conditions before summer drought (i.e., in spring), and their carry-over impacts on summer drought, and also when it comes to the quantification of spring carry-over effects and summer drought effects across different carbon cycle data sets.

In this study, we revisit the 2012 drought and also the 2011 drought in North America, studying their impacts on terrestrial carbon fluxes with an ensemble of carbon flux estimates and remotely sensed hydroclimate and vegetation activity. To constrain uncertainties in modeled carbon fluxes, we use a range of carbon flux data sets or models, including in situ flux upscaled data set (i.e., a data-driven model, FLUXCOM), TBMs (TRENDY DGVMs and SiBCASA), and atmospheric inversions (CarbonTracker Europe [CTE] 2016 and CarbonTracker [CT] 2016). The employed remotely sensed metrics include Global Land-surface Evaporation Amsterdam Methodology (GLEAM) root-zone SM, Gravity Recovery and Climate Experiment (GRACE) terrestrial TWS, Global Ozone Monitoring Experiment-2 (GOME-2) solar-induced fluorescence, and Moderate Resolution Imaging Spectroradiometer (MODIS) enhanced vegetation index (EVI). This study aims to answer the following scientific questions: (1) What was the direction and magnitude of net carbon uptake anomalies during two large-scale North American summer droughts in 2011 and 2012? (2) How did individual processes

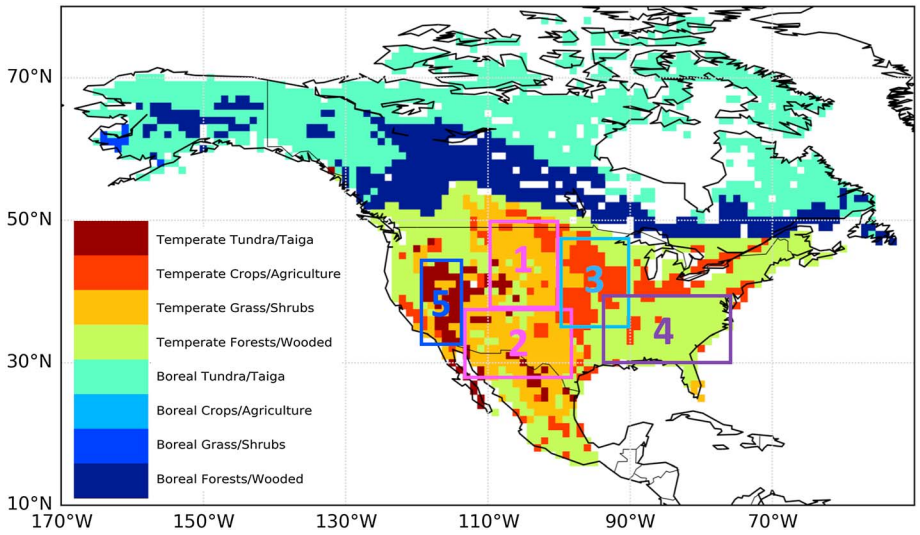

Figure 1. The aggregated ecoregions based on Olson ecosystem classification and Transcom land regions of North America and the subregions (R1–R5) used for analysis of the impact of droughts.

(GPP and Reco) contribute to these anomalies, and which role did the unusually cold (warm) spring in 2011 (2012) prior to drought play in determining the interplay of GPP and Reco? (3) How did spatial patterns and individual ecoregions contribute to these net carbon uptake anomalies?

2. Data and Methods

2.1. Study Area

North America spans 10–80°N, 175–55°W, including Canada, the United States, and Mexico. We divided the study area into different ecoregions based on the Olson ecosystem classification (Olson et al., 2000) and Transcom land regions (Gurney et al., 2004). These ecoregions (Figure 1) include four classes for both boreal and temperate zones: grass/shrubs, crops/agriculture, forests/wooded, and tundra/taiga. As most drought events occur in temperate North America, we focused the analysis over five selected subregions across the midlatitudes (Figure 1). In addition, we used the Köppen-Geiger climate zone classification (Kottek et al., 2006; Rubel et al., 2017; supporting information Figure S1) to delineate arid and semiarid areas.

2.2. CO_2 Fluxes

In order to constrain the uncertainties in the analysis of carbon flux variability, we employed an ensemble of state-of-the-art CO_2 flux products, including FLUXCOM, TRENDY DGVMs, SiBCASA, CTE2016, and CT2016. CO_2 flux data, satellite land surface data, and meteorological data used in this study are summarized in Table 1 and are introduced in the following sections.

2.2.1. FLUXCOM

The FLUXCOM product is based on upscaled FLUXNET CO_2 flux measurements. Upscaling uses ML algorithms (Jung et al., 2017; Tramontana et al., 2016) to scale in situ CO_2 flux measurements into time-resolved $0.5° \times 0.5°$ grids of NEP, Reco, and GPP for the period 1980–2013 using meteorological data and mean seasonal cycles of remotely sensed data. Meteorological variables were retrieved from the CRUNCEP v6 data set. The distribution of plant functional types originates from the majority class of annually resolved MODIS land cover product (collection 5; Friedl et al., 2010). The daily fluxes were finally aggregated to monthly values. Predictions of GPP and Reco fluxes were performed with three different ML algorithms, including artificial neural networks, multivariate adaptive regression splines, and random forests, and two methods used for separating GPP and Reco from tower-based NEP (Lasslop et al., 2010; Reichstein et al., 2005). Thus, there are six sets of GPP and Reco, respectively, and a total of 36 sets of NEP by combining these GPP and Reco data sets. In this study, we used the means and standard deviations of different NEP, GPP, and Reco data sets over the period from 2007 to 2013 for analysis.

Table 1
Specifics of the CO_2 Fluxes, Meteorological Data, and Satellite Land Surface Data Used in This Study

Products	Spatial resolution	Temporal resolution	Time span	References
FLUXCOM	0.5° × 0.5°	Monthly	1980–2013	Tramontana et al. (2016); Jung et al. (2017)
TRENDY DGVMs	0.5° × 0.5°	Monthly	Diverse, including 2007–2014	Sitch et al. (2015)
SiBCASA	1° × 1°	3-hourly	2000–2014	van der Velde et al. (2014)
CTE2016	1° × 1°	Monthly	2000–2015	van der Laan-Luijkx et al. (2017)
CT2016	1° × 1°	Monthly	2000–2015	Peters et al. (2007)
CRUNCEP	0.5° × 0.5°	6-hourly	1901–2013	New et al. (2000)
GLEAM v3.1a	0.25° × 0.25°	Monthly	1980–2016	Martens et al. (2017)
GRACE TWS	1° × 1°	Monthly	2000–2014	Swenson and Wahr (2006); Landerer and Swenson (2012)
GOME-2 SIF	0.5° × 0.5°	Monthly	2007–2016	Joiner et al. (2013)
MODIS EVI	0.05° × 0.05°	16 days	2000–2016	Huete et al. (2002)

Note. DGVMs = dynamic global vegetation models; SiBCASA = combined Simple Biosphere/Carnegie-Ames-Stanford Approach; CTE = CarbonTracker Europe; CT = CarbonTracker; GLEAM = Global Land-surface Evaporation Amsterdam Methodology; GRACE TWS = Gravity Recovery and Climate Experiment total water storage; GOME-2 SIF = Global Ozone Monitoring Experiment-2 solar-induced chlorophyll fluorescence; MODIS EVI = Moderate Resolution Imaging Spectroradiometer enhanced vegetation index.

2.2.2. TRENDY DGVMs

Monthly carbon fluxes (GPP, autotrophic respiration, and heterotrophic respiration) at a spatial resolution of 0.5° × 0.5° simulated by six DGVMs from the TRENDY project (version 5, simulation S2; Sitch et al., 2015) were used here. These models include ORCHIDEE (Krinner et al., 2005), CABLE (Y. Wang et al., 2010), DLEM (Tian et al., 2015), ISAM (Jain et al., 2013), VEGAS (Zeng et al., 2005), and VISIT (Kato et al., 2013). They were all driven by the CRUNCEP v7 data set (https://vesg.ipsl.upmc.fr/thredds/catalog/store/p529viov/cruncep/V7_1901_2015/catalog.html). Outputs from the TRENDY project have been widely employed to study the terrestrial carbon cycle at regional and global scales (Ahlström et al., 2015; Bastos et al., 2016; Jung et al., 2017; Le Quéré et al., 2016; Piao et al., 2013; Sitch et al., 2015).

2.2.3. The Combined Simple Biosphere/Carnegie-Ames-Stanford Approach

The SiBCASA model (Schaefer et al., 2008) is a combination of the Simple Biosphere (SiB) model (Baker et al., 2008; Sellers et al., 1996) and the Carnegie-Ames-Stanford Approach (CASA) model (Potter et al., 1993). This study used the simulation with improved biomass burning fluxes following van der Velde et al. (2014). The meteorological drivers were retrieved from the European Centre for Medium-Range Weather Forecasting data set. We used the simulated carbon fluxes at a spatial resolution of 1° × 1° and a temporal resolution of 3 hr.

2.2.4. CarbonTracker Europe

The CTE (Peters et al., 2010; van der Laan-Luijkx et al., 2017) developed at Wageningen University assimilates global air samples of CO_2 mole fractions to constrain prior surface carbon fluxes simulated by the SiBCASA model. The CTE data set has been widely applied in carbon cycle studies (Le Quéré et al., 2016; Thompson et al., 2016). Recently, Wolf et al. (2016) used the CTE products (CTE2014 and CTE2015) to study the response of carbon fluxes to the 2012 drought over south Great Plains in the United States. Here we used the monthly CTE2016 data set with a spatial resolution of 1° × 1°.

2.2.5. CarbonTracker

Another atmospheric CO_2 inversion product from CT2016 (Peters et al., 2005; Peters et al., 2007) developed at the National Oceanic and Atmospheric Administration was also employed in this study. The differences between CTE2016 and CT2016 were illustrated by van der Laan-Luijkx et al. (2017) in detail. The most important differences are as follows: CTE2016 uses gridded state vector, while CT2016 uses ecoregion state vector; they use different prior fluxes for biosphere, ocean, fires, and fossil fuels; and they use different subsets of CO_2 observations. We used the monthly CT2016 data set at a spatial resolution of 1° × 1°.

2.3. Satellite Land Surface Data

Relative to most carbon cycle models, satellite observations provide more direct and uniform information about land surface and thus are valuable for identifying spatiotemporal anomalies in hydrological and vegetation status. Four remote sensing metrics were chosen to indicate hydrological conditions and vegetation activities: root-zone SM, terrestrial TWS, solar-induced fluorescence, and EVI. All those metrics can be used to indicate drought conditions; and SIF also is often used as a proxy for GPP.

2.3.1. GLEAM SM

The GLEAM root-zone SM v3.1a data was inferred from the satellite surface SM product ESA-CCI SM (v02.5) by data assimilation (Martens et al., 2017; Miralles et al., 2011). ESA-CCI SM is a satellite SM product from the European Space Agency Climate Change Initiative and an Essential Climate Variable, which is a combination of passive (SMMR, SSM/I, TMI, AMSR-E, WindSat, AMSR2, and SMOS) and active (AMI-WS and MetOp A/B ASCAT) microwave products with a spatial resolution of 0.25° × 0.25° (Dorigo et al., 2017). The data set has been validated against in situ measurements by many studies (Dorigo et al., 2015; Peng et al., 2015). By assimilating the ESA-CCI SM data, GLEAM SM (v3.1a) has a better spatial continuity and also higher correlation with carbon flux anomalies indicated in our experimental comparison; hence, we used the GLEAM SM data in our analysis.

2.3.2. GRACE TWS

GRACE reveals dynamics of terrestrial TWS over the globe through observing temporal gravity field variations. The 1° × 1° GRACE Level-2 RL05 TWS data were downloaded from NASA's GRACE Tellus website (http://podaacftp.jpl.nasa.gov/allData/tellus/L3/land_mass/RL05/) over North America for the period from 2007 to 2014 (Landerer & Swenson, 2012; Swenson & Wahr, 2006). To minimize the uncertainties associated with data preprocessing, the product used ensemble means of the available three GRACE-TWS products preprocessed independently by three research centers: NASA Jet Propulsion Laboratory, University of Texas Center for Space Research, and the GeoForschungsZentrum Potsdam. In this product, scaling coefficients from the National Center for Atmospheric Research's CLM 4.0 model (Gent et al., 2011) were adopted to correct and restore the GRACE signal attenuation due to filtering (Xie et al., 2016).

2.3.3. GOME-2 SIF

SIF has shown great promise for probing spatiotemporal variations of GPP (Guanter et al., 2014; Zhang et al., 2016) and is also sensitive to water stress (Alden et al., 2016; Lee et al., 2013; Sun et al., 2015). The monthly SIF at 740 nm with a spatial resolution of 0.5° × 0.5° (version 26) retrieved from the GOME-2 (Joiner et al., 2013) was used to indicate vegetation activity specifically on photosynthetic CO_2 uptake under droughts or temperature anomalies.

2.3.4. MODIS EVI

Complementary to SIF, EVI from the MODIS product MOD13C1 was also used to indicate vegetation response to droughts and temperature anomalies. This 16-day composite data set at a spatial resolution of 0.05° × 0.05° was calculated using the MODIS/Terra reflectance (v6) data (Huete et al., 2002). A Savitzky-Golay filter built in the TIMESAT 3.2 software (Jönsson & Eklundh, 2004) was applied to filter low-quality data.

2.4. Meteorological Data

In order to disentangle the drought impact from the combined effect of water and temperature anomalies on carbon fluxes, we included air temperature data in our analysis. Precipitation data can also be used as a reference for satellite hydrological metrics. We used monthly air temperature and precipitation data at a spatial resolution of 0.5° × 0.5° from the CRUNCEP v6 data set produced by the Institute Pierre Simon Laplace of France (Wei et al., 2014). CRUNCEP v6 is a merged product of Climate Research Unit observation-based monthly 0.5° × 0.5° climate variables (New et al., 2000; 1901–2014) and the 6-hourly high-resolution reanalysis of National Centers for Environmental Prediction. This data set is also the meteorological driver of the FLUXCOM and TRENDY products.

2.5. Analysis Methods

2.5.1. Calculation of Anomalies

The anomalies of carbon fluxes and meteorological, hydrological, and vegetation metrics were calculated as follows:

$$X_i^{'} = X_i - \overline{X_{\mathrm{BL}}} \tag{1}$$

where $X_i^{'}$ is the anomaly of variable X in the ith month or year. X_i denotes the value of variable X in the ith month or year, and $\overline{X_{\mathrm{BL}}}$ is the mean of variable X in months or years during a baseline period. Following Wolf et al. (2016), we took the period from 2008 to 2010, when climate conditions were relatively harmonious, as the baseline.

2.5.2. Correlation Analysis

Pearson's correlation was used as a measure of association between anomalies of meteorological or hydrological metrics and carbon fluxes. All data sets were processed to consistent 0.5° × 0.5° grids and monthly

Table 2
Terrestrial Carbon Fluxes of North America During 2007–2014 From 10 Models (Unit: Pg C/year)

Fluxes	Models	2007	2008	2009	2010	2011	2012	2013	2014	Mean	STD	CV
GPP	FLUXCOM	15.65	15.66	15.59	15.78	15.54	15.55	15.69	-	15.64	0.09	0.01
	SiBCASA	17.58	17.53	17.28	18.29	17.57	17.82	17.25	17.57	17.61	0.33	0.02
	ORCHIDEE	24.70	24.99	24.47	26.19	24.74	25.53	25.60	26.10	**25.29**	0.66	0.03
	CABLE	18.08	18.51	18.18	18.84	18.17	18.63	18.56	18.61	18.45	0.27	0.01
	DLEM	14.87	14.25	14.02	15.08	14.23	15.17	14.52	14.55	**14.59**	0.42	0.03
	ISAM	17.78	17.45	17.07	18.26	17.68	18.03	18.02	18.43	17.84	0.44	0.02
	VEGAS	15.55	14.90	14.84	15.51	15.07	15.74	15.15	15.47	15.28	0.33	0.02
	VISIT	18.81	18.57	18.56	19.08	18.60	19.01	18.92	19.69	18.90	0.38	0.02
	Mean	17.88	17.73	17.50	18.38	17.70	18.19	17.96	18.63	17.95	-	-
	STD	3.09	3.35	3.23	3.54	3.26	3.32	3.48	3.76	3.36	-	-
Reco	FLUXCOM	12.64	12.52	12.51	12.77	12.57	12.72	12.65	-	**12.62**	0.10	0.01
	SiBCASA	17.25	17.20	17.11	17.83	17.35	17.51	17.17	17.26	17.34	0.23	0.01
	ORCHIDEE	23.81	23.65	23.53	24.66	24.00	24.64	24.21	24.63	**24.14**	0.46	0.02
	CABLE	16.59	16.40	16.43	16.98	16.59	17.12	16.59	16.66	16.67	0.25	0.02
	DLEM	14.50	14.02	13.97	14.70	14.35	14.79	14.20	14.30	14.35	0.30	0.02
	ISAM	17.20	16.70	16.58	17.75	17.48	17.95	17.32	17.63	17.33	0.48	0.03
	VEGAS	15.08	14.56	14.49	15.11	14.76	15.24	14.72	14.95	14.86	0.27	0.02
	VISIT	17.48	17.37	17.56	18.12	17.67	18.06	17.73	18.18	17.77	0.31	0.02
	Mean	16.82	16.55	16.52	17.24	16.85	17.25	16.82	17.66	16.89	-	-
	STD	3.29	3.34	3.32	3.54	3.41	3.51	3.48	3.38	3.43	-	-
NEP	FLUXCOM	3.01	3.14	3.08	3.02	2.96	2.83	3.04	-	**3.01**	0.10	0.03
	SiBCASA	0.33	0.33	0.17	0.46	0.23	0.31	0.08	0.30	0.27	0.12	0.42
	ORCHIDEE	0.89	1.34	0.93	1.53	0.74	0.90	1.39	1.47	1.15	0.31	0.27
	CABLE	1.49	2.11	1.76	1.86	1.58	1.51	1.98	1.95	1.78	0.23	0.13
	DLEM	0.37	0.23	0.04	0.39	−0.12	0.38	0.32	0.25	**0.23**	0.18	0.78
	ISAM	0.58	0.74	0.49	0.51	0.20	0.08	0.70	0.80	0.51	0.26	0.50
	VEGAS	0.47	0.34	0.35	0.40	0.31	0.50	0.43	0.52	0.42	0.08	0.19
	VISIT	1.34	1.21	0.99	0.96	0.93	0.95	1.19	1.51	1.13	0.21	0.19
	CTE2016	1.00	0.71	0.81	0.96	0.81	0.79	0.66	0.86	0.82	0.11	0.14
	CT2016	0.86	0.35	0.94	0.92	0.67	0.50	0.66	0.91	0.73	0.22	0.30
	Mean	1.03	1.05	0.96	1.10	0.83	0.87	1.04	0.95	1.01	-	-
	STD	0.80	0.94	0.89	0.83	0.89	0.80	0.90	0.58	0.85	-	-

Note. Bold signifies maximum or minimum values. STD = standard deviation; CV = coefficient of variation; CTE = CarbonTracker Europe; CT = CarbonTracker.

time steps for correlation calculations. We considered lagged effects for hydrological variables (precipitation, SM, and TWS) and cumulative effects for precipitation. To calculate maximum correlation coefficients, anomalies of precipitation, SM, and TWS in each grid were chosen as those with a backward shift of several months (0 to 12 months) to correlate anomalies of carbon fluxes in the current month; precipitation was additionally used as the mean of those in two previous months (Eisfelder et al., 2014; Yang et al., 2014).

3. Results

3.1. Annual Anomalies of Carbon Fluxes During 2007–2014 and Links to Climatic Factors

3.1.1. Annual Anomalies of GPP, Reco, and NEP During 2007–2014

Overall, terrestrial ecosystems in North America act as a carbon sink for the period 2007–2014 but with large discrepancies in magnitudes of carbon fluxes estimated by different models (Table 2). These models were classified into three categories: data-driven FLUXCOM, TBMs (DGVMs and SiBCASA), and AIMs (CTE2016 and CT2016). The annual means of NEP range from 0.23 (DLEM) to 3.01 Pg C/year (FLUXCOM), with an ensemble estimate of 1.01 ± 0.85 Pg C/year. The annual means of GPP range from 14.59 (DLEM) to 25.29 Pg C/year (ORCHIDEE), with an ensemble estimate of 17.95 ± 3.36 Pg C/year. The annual means of Reco range from 12.62 (FLUXCOM) to 24.14 Pg C/year (ORCHIDEE), with an ensemble estimate of 16.89 ± 3.43 Pg C/year. Among these models, FLUXCOM simulates lowest means and interannual variations (IAVs) of GPP and Reco, which is consistent with previous findings regarding similar data sets (Anav et al., 2013; Kumar et al.,

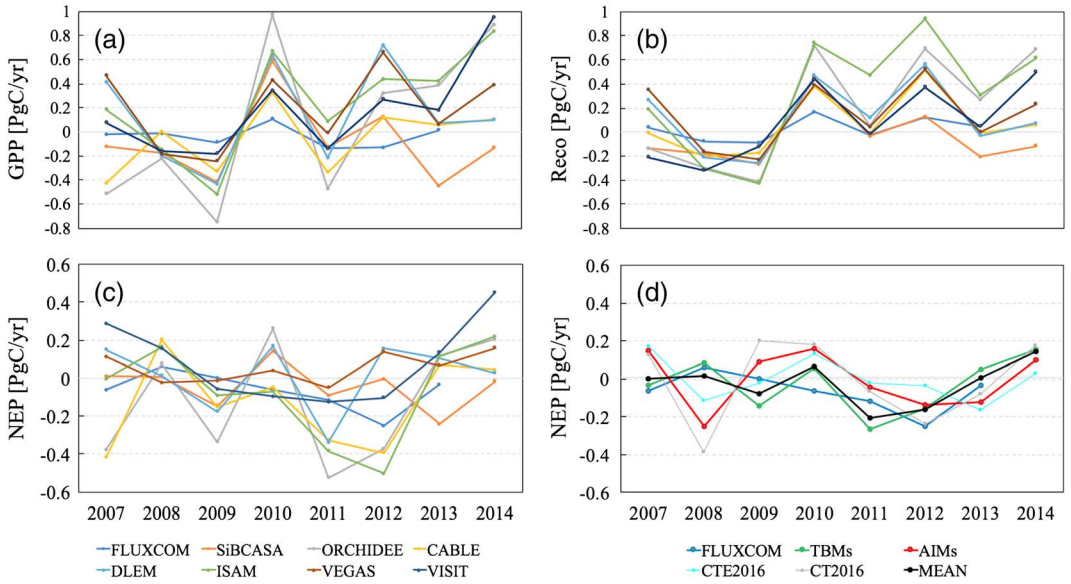

Figure 2. Annual anomalies of GPP, Reco, and NEP (Pg C/year) relative to the baseline period 2008–2010 from an ensemble of carbon cycle models in North America during 2007–2014. *TBMs* indicates the mean of DGVMs and SiBCASA; *AIMs* indicates the mean of CTE2016 and CT2016; *MEAN* is the mean of all used carbon models. GPP = gross primary production; NEP = net ecosystem production; DGVMs = dynamic global vegetation models.

2016; Piao et al., 2013). FLUXCOM simulates much larger NEP than TBMs and AIMs but with the lowest IAV indicated by the standard deviation (as expected from earlier studies with data-driven models). The 8-year average NEP estimated by the two AIMs is close to the ensemble mean, while NEP simulated by TBMs are divergent, ranging from 0.27 (SiBCASA) to 1.78 Pg C/year (CABLE). In summary, there is still a large discrepancy in the magnitudes and IAV of carbon fluxes estimated by different models.

However, flux anomalies derived from different carbon models are generally consistent in signs over time (Figure 2 and Table S1). GPP and Reco show relatively large IAV, whereas NEP has much smaller variations with substantial declines in 2011 and 2012 indicated by the ensemble means. The model ensemble suggests an annual average increase of GPP (0.09 ± 0.26 Pg C/year) and Reco (0.12 ± 0.19 Pg C/year) and as a result a slight decrease of NEP (−0.03 ± 0.08 Pg C/year) relative to the period 2008–2010 during 2007–2014 in North America (Table S1). Annual NEP anomalies over the study area depend on the magnitudes and signs of GPP and Reco anomalies (Figures 2a–2c). For 2010 and 2014, both GPP and Reco are clearly larger than those during the baseline period; the former increases more than the latter, resulting in NEP above the baseline. For 2011 and 2012, although variations in GPP and Reco were different, NEP decreases in similar magnitudes indicated by the ensemble mean. It should be noted that the NEP anomalies of 2011 and 2012 derived from different models exhibit large discrepancies (Figures 2c and 2d); the two atmospheric inversions show much smaller NEP reduction than TBMs in 2011, which is mainly contributed by the inconsistent positive anomaly during the summer (see Figure 5). Despite the discrepancies, all the three categories of models (Figure 2d) show a considerable reduction of NEP in both years.

We further investigated annual anomalies of GPP, Reco, and NEP across different ecoregions (Figure 3) using TBMs only. On the whole, a large negative anomaly is observed in the temperate area with a small negative NEP anomaly in the boreal area, indicating that the temperate area was mainly responsible for the North American NEP reductions over 2007–2014. In addition, large anomalies of GPP and Reco are observed in both areas. Compared to the boreal area, the temperate area shows less increase on GPP but more on Reco. In the boreal area, forests/wooded and grass/shrubs show negative NEP anomalies, while tundra/taiga shows a positive NEP anomaly. The forests/wooded shows a negative NEP anomaly due to larger increase of Reco than that of GPP while inversely for tundra/taiga. From a regional perspective, the positive NEP anomaly in tundra/taiga compensates the negative anomaly caused by forests/wooded. In contrast, the temperate area shows evident negative NEP anomalies, being responsible by the large NEP reductions of grass/shrubs and

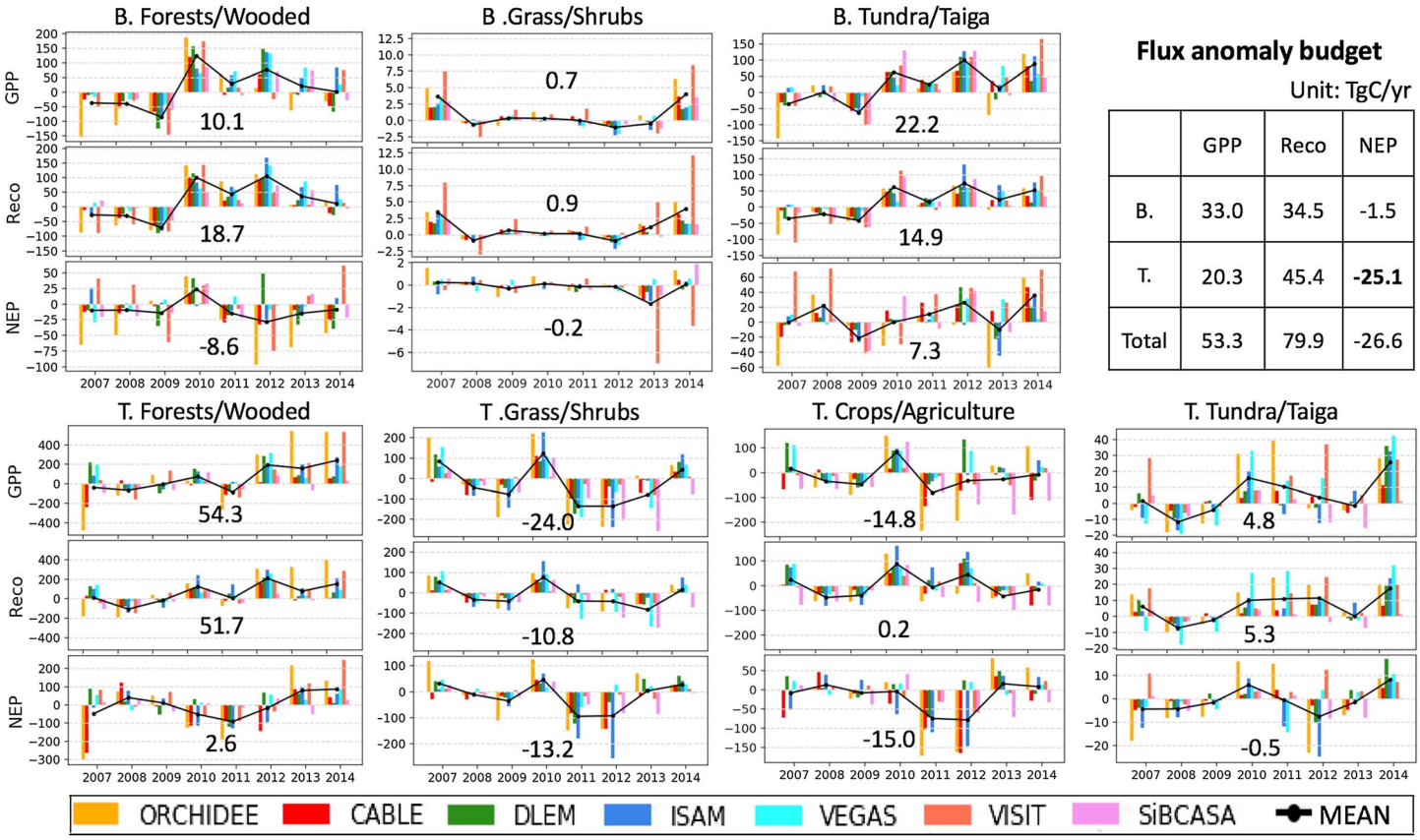

Figure 3. Annual anomalies of GPP, Reco, and NEP relative to the baseline period 2008–2010 from an ensemble of carbon cycle models (TRENDY DGVMs and SiBCASA) for seven ecoregions in North America during 2007–2014. *B.* and *T.* are short for *boreal* and *temperate*, respectively. The numbers in subgraphs indicate total flux anomalies in ecoregions. Largest anomalies of NEP took place in the temperate grass/shrubs and crops/agriculture, especially in 2011 and 2012. GPP = gross primary production; NEP = net ecosystem production; DGVMs = dynamic global vegetation models.

crops/agriculture in 2011 and 2012 associated with severe droughts (also see Figure 6b). The GPP reductions in these two ecoregions dominate the negative anomalies of North American NEP. However, the forests/wooded plays a positive role in the North American NEP anomalies, which was also reported by Wolf et al. (2016).

3.1.2. Geographical Connection Between Carbon Flux Anomalies and Climatic Factors

To geographically attribute the carbon flux anomalies, we calculated the Pearson's correlation coefficients between monthly anomalies of carbon fluxes and meteorological or hydrological metrics over the period 2007–2014 at the grid scale (Figure 4) and at subregion and continental scales (Figure S2), respectively.

Pearson's correlation coefficients between monthly anomalies of GPP estimated by different models and meteorological or hydrological metrics are presented in Figure 4. Air temperature highly correlates to GPP, especially in the boreal area, as estimated by FLUXCOM, DGVMs (taking the ensemble mean), and SiBCASA. However, high air temperature anomalies could cause GPP reduction in the southern end area, such as Texas, as indicated by FLUXCOM, DGVMs, and SiBCASA. In contrast, GPP in FLUXCOM, DGVMs, and SiBCASA are positively correlated with hydrological indicators (precipitation, SM, and TWS) in the semiarid Southwest and Great Plains, which are frequently hit by droughts, suggesting that these areas are mostly responsible for carbon flux anomalies. In addition, indicated by the lagged months (time scales) of maximum correlations between anomalies of GPP and hydrological indicators, the Southwest quickly responds to hydrological anomalies, while the north (mostly the boreal area) responds slower, at about 8–10 months on average. This indicates that the hydrological conditions in the Southwest have a strong impact on North American carbon fluxes and different biomes respond to droughts with different time scales. We also performed similar analysis for the estimated NEP from CTE2016 and CT2016 and found that they correlated

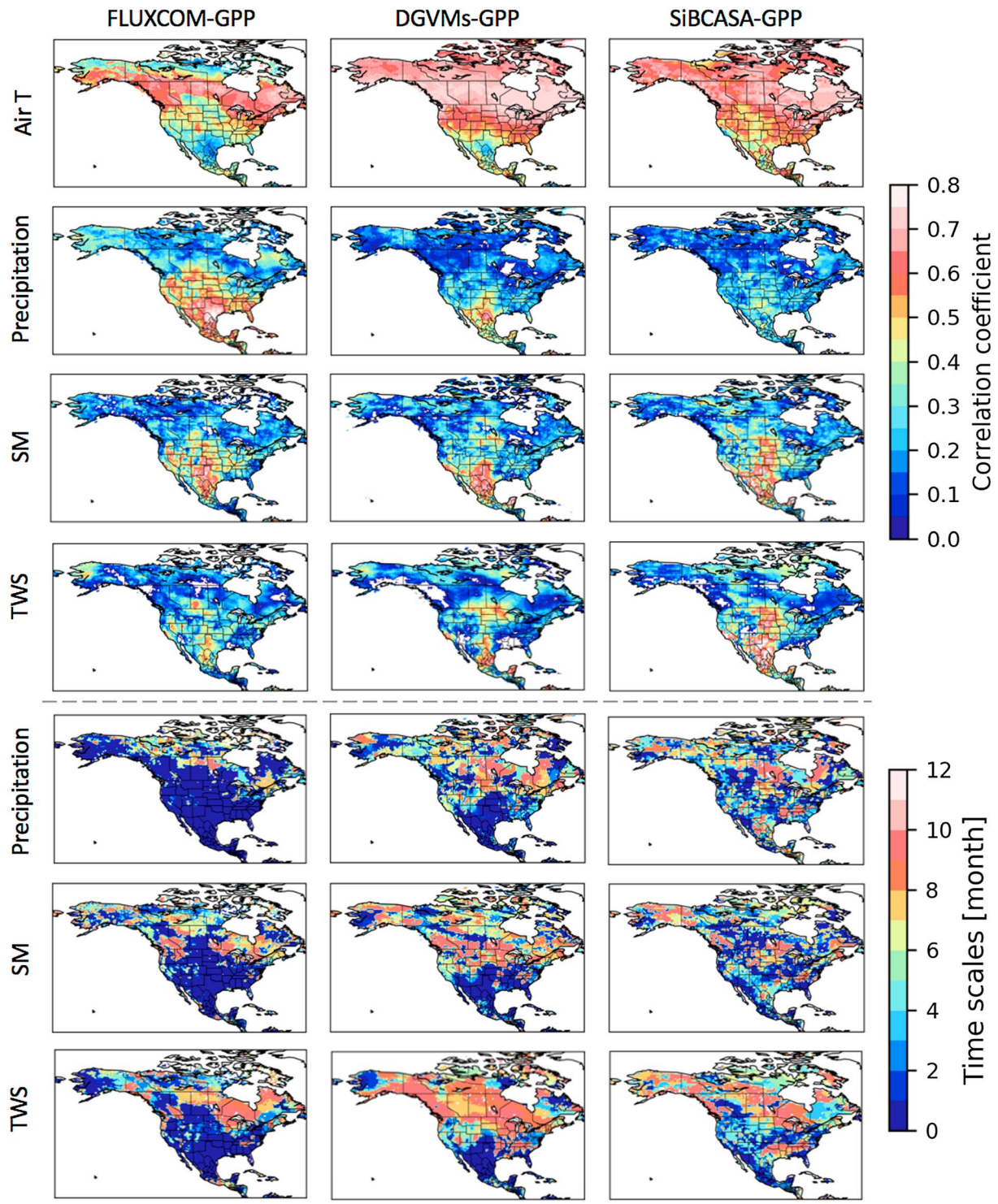

Figure 4. Pearson's correlation coefficients between anomalies of GPP (estimated by FLUXCOM, DGVMs, and SiBCASA) and meteorological and hydrological metrics (air temperature, air T; precipitation; soil moisture, SM; terrestrial total water storage, TWS) during the period 2007–2014. For air temperature, it was calculated in time of the current month; for others, maximum correlation coefficient was calculated with consideration of lagged effect with up to 12 months. GPP = gross primary production; DGVMs = dynamic global vegetation models.

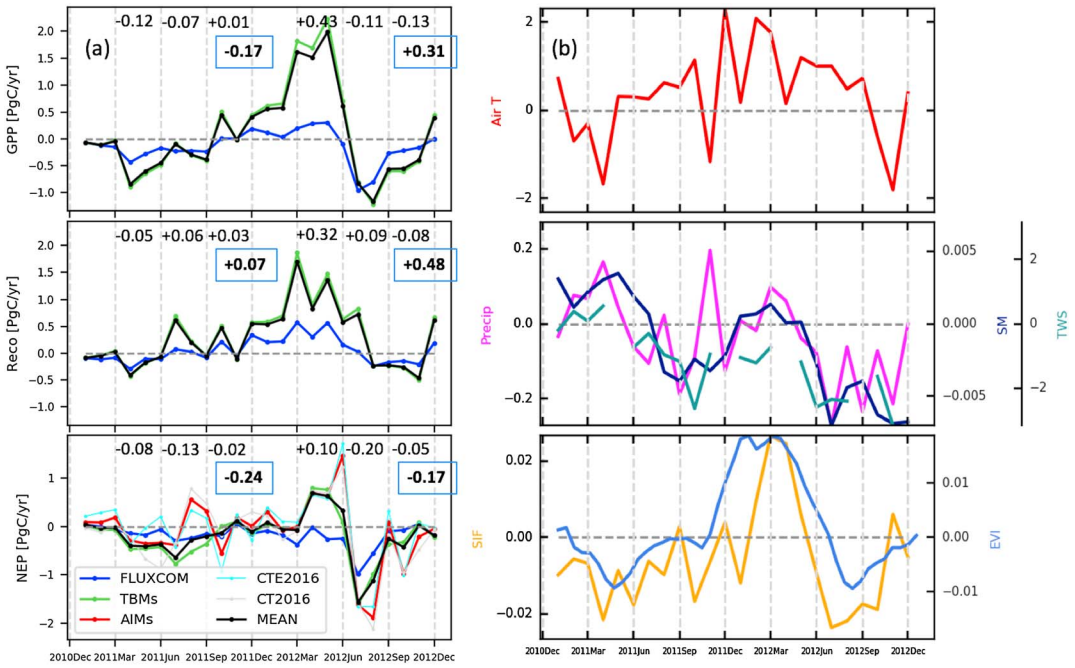

Figure 5. Monthly (16-day for EVI) anomalies of carbon fluxes, air temperature, and hydrological and vegetation metrics relative to the baseline period 2008–2010 in 2011 and 2012: (a) GPP, Reco, and NEP (Pg C/year) from an ensemble of carbon cycle models. The numbers with positive or negative signs are increased or decreased fluxes for spring, summer, fall, and annual total (with blue rectangles). *MEAN* is the mean of all used carbon models; (b) air temperature (air T, °C), precipitation (mm), SM (m^3/m^3), TWS (mm), SIF ($mW/m^2/nm/sr$), and EVI (unitless) during 2011–2012. EVI = enhanced vegetation index; GPP = gross primary production; NEP = net ecosystem production SM = soil moisture; TWS = total water storage; SIF = solar-induced chlorophyll fluorescence.

weakly with these metrics of meteorology and hydrology at grid scale (not shown). This is due to the fact that the two data sets have limited spatial details since limited atmospheric CO_2 observations were used for constraining grid-scale carbon fluxes.

We further calculated correlations on the regional scale for GPP, Reco, and NEP fluxes that included the two atmospheric inversions for the five subregions (Figure S2). SM and TWS show evidently positive correlations with carbon fluxes in most regions. The results of FLUXCOM, DGVMs, and SiBCASA consistently indicate that the increase of air temperature has larger influences on Reco than GPP and contribute to negative correlations with NEP in all regions (especially in FLUXCOM data). Weak effects of air temperature on regional carbon fluxes are indicated by CTE2016 and CT2016. Despite large discrepancy among different models, air temperature has a stronger influence on Reco than GPP over North America. The NEP of CTE2016 and CT2016 exhibit good correlations with precipitation and SM but do not correlate well with TWS. On the whole, CTE2016 shows better correlation with these metrics than CT2016. On the regional scale overall, carbon flux anomalies highly correlate to the hydrological anomalies. Compared to GPP and Reco, NEP shows lower correlations with these EO, which might be explained by the relative larger uncertainties in simulating NEP than GPP and Reco and mutual compensation of GPP and Reco (Jung et al., 2017).

3.2. Process and Spatiotemporal Attribution of NEP Reductions in 2011 and 2012

3.2.1. Continental Scale

In 2011 and 2012, evident reductions of NEP with similar magnitudes (Table S1) but different underlying mechanisms occurred (Table S2). The NEP reduction of −0.24 ± 0.17 Pg C/year (−0.20 ± 0.17 Pg C/year if including two atmospheric inversions) in 2011 arises due to a moderate decrease of GPP (−0.17 ± 0.18 Pg C/year) and a small increase of Reco (+0.07 ± 0.17 Pg C/year), while the NEP reduction of −0.17 ± 0.25 Pg C/year (0.16 ± 0.23 Pg C/year if including two atmospheric inversions) in 2012 is owing to a larger increase of Reco (+0.48 ± 0.27 Pg C/year) than that of GPP (+0.31 ± 0.29 Pg C/year).

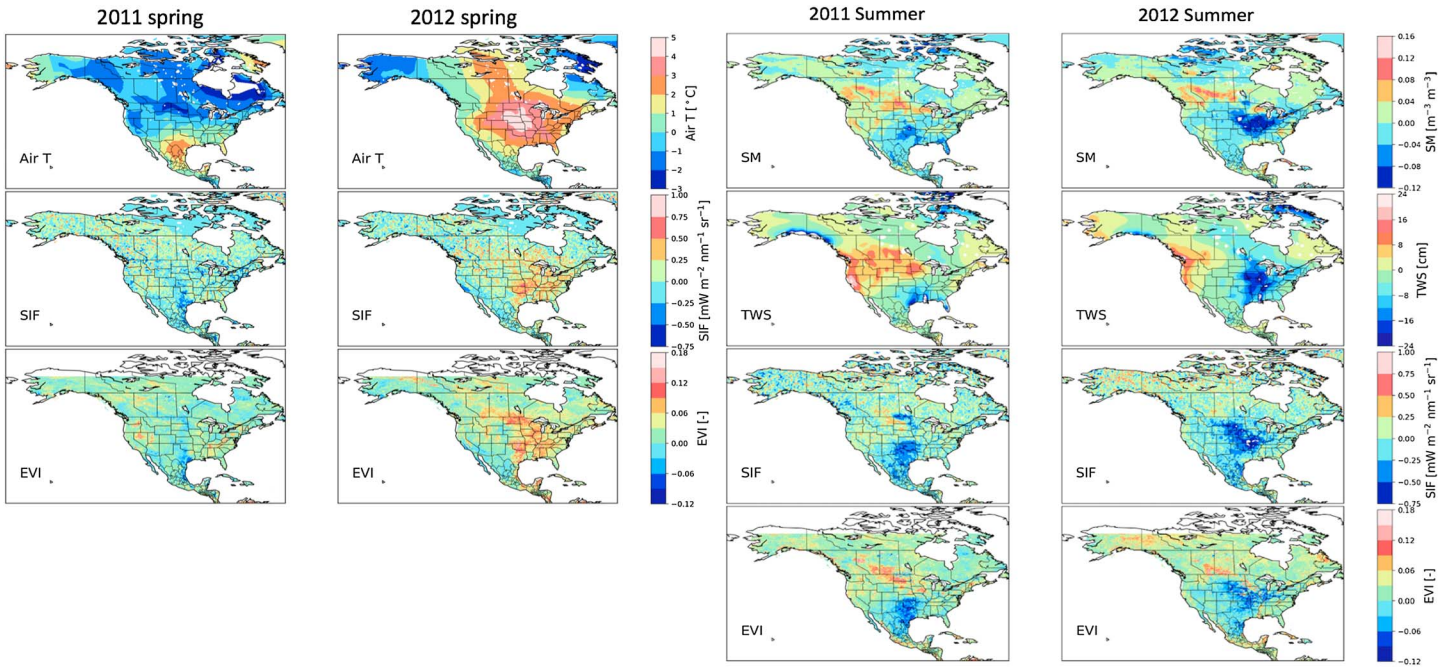

Figure 6. Spatial distribution of spring (March–May) temperature anomalies and summer (June–August) droughts and vegetation responses in 2011 and 2012.

Each drought year also had a unique pattern of seasonal anomalies (Figure 5a). In 2011, the ensemble mean anomalies of monthly NEP were continuously negative during April–October, resulting in a reduction of 0.24 Pg C/year in annual NEP. In 2012, accumulated NEP was 0.10 Pg C/year above the baseline from April to June and then was 0.25 Pg C/year smaller than the baseline from July to October, contributing to the annual NEP decline of 0.17 Pg C/year. Despite the difference in magnitudes, FLUXCOM and TBMs exhibit consistent signs of seasonal variations of GPP and Reco in 2011 and 2012. In general, the three categories of models exhibit consistent patterns in seasonal variations of NEP; however, the variation magnitude of FLUXCOM is least, while those of AIMs are largest. Also, clear differences of NEP anomalies between AIMs and the others are observed, for example, in the 2011 summer and the late spring-early summer of 2012. For the former period, it is not certain whether this is mainly due to the uncertainty from atmospheric inverse modeling or terrestrial biosphere modeling, but available evidences tend to support the latter. That is because it is unlikely that Reco reduces much stronger than GPP (shows a reduction indicated by SIF) over North America under drought and high-temperature conditions in summer if it is the case indicated by AIMs. Meanwhile, it is possible that there are some CO_2 emissions due to drought that have not been well quantified in the inversions, and thus an enhanced net carbon uptake has been estimated. The meteorological, hydrological, and vegetation metrics helped to track seasonal climate anomalies and to attribute NEP reductions (Figure 5b). The anomalies of precipitation, SM, and TWS coincide with each other, especially during the drought periods of 2011 and 2012. The anomalies of SIF and EVI agree well with each other and GPP over time, clearly identifying the vegetation responses to summer droughts and spring temperature anomalies.

In the two drought years, the model ensemble indicates that GPP reduced but Reco increased during both summers on the continental scale. The summer drought in 2012 negatively affected carbon sequestration as GPP decreased more so than Reco. NEP was obviously lower than the baseline period during July–October of 2012. Starting from July, GPP declined sharply (about 0.24 Pg C/year) owing to the drought, while Reco decreased less (about 0.08 Pg C/year) and later. This is a typical pattern during droughts (Schwalm et al., 2010; von Buttlar et al., 2018). The ensemble mean of FLUXCOM and TBMs indicates that the response of Reco to drought was lagged and lasted longer in comparison with that of GPP. The largest reduction of NEP occurred in July when high temperature and drought co-occurred, since GPP sharply declined while Reco kept increasing suggested by the ensemble mean of TBMs. In 2011, the largest NEP reduction also occurred in July which mostly contributed by positive Reco anomaly. Compared to the drought effect in

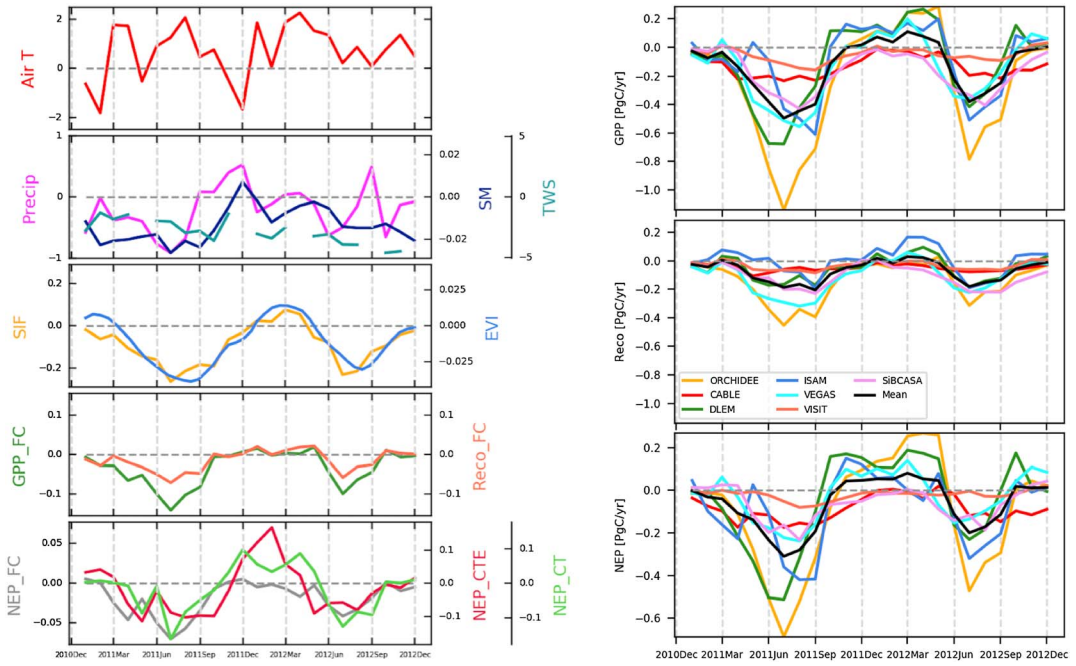

Figure 7. Monthly (16-day for EVI) anomalies of air temperature, hydrological and vegetation metrics, and carbon fluxes for Region 2 (grass/shrubs, southern) of North America in 2011 and 2012. (left column) Air temperature (air T, °C), precipitation (mm), SM (m^3/m^3), TWS (cm), SIF ($mW/m^2/nm/sr$), and EVI (unitless), and GPP, Reco and NEP from FLUXCOM (labeled with *FC*), CTE2016 and CT2016; (right column) GPP, Reco, and NEP from an ensemble of DGVMs. The unit of carbon flux is Pg C/year. EVI = enhanced vegetation index; SM = soil moisture; TWS = total water storage; SIF = solar-induced chlorophyll fluorescence; GPP = gross primary production; NEP = net ecosystem production; DGVMs = dynamic global vegetation models.

2012, the 2011 summer drought caused much smaller flux seasonal anomalies of GPP and NEP, which could be explained by a smaller influence extent.

The spring warming in 2012 enhanced carbon sequestration, which partly offset the negative impact of the summer drought on annual NEP (see also Wolf et al. (2016)). In contrast, in 2011, abnormally lower air temperature caused GPP and Reco to decrease considerably during April–June, the former at a larger magnitude than the latter (see Table S2), resulting in the clear annual NEP reduction. Therefore, warmer spring is beneficial to carbon sequestration by terrestrial ecosystems in North America. However, it should be noted that possible negative effect of spring warming can jeopardize summer water availability (discussed in section 4.1).

To further spatially attribute the carbon flux anomalies (refer to Figure S3), we mapped the anomalies of air temperature, hydrology (SM and TWS), and vegetation activity (SIF and EVI) during the springs (March–May) and summers (June–August) of 2011 and 2012 (Figure 6). Anomalies of hydrological and vegetation metrics show consistent spatial patterns in 2011 and 2012, respectively. These metrics indicate that drought occurred mainly in Texas and Mexico in 2011, while it mainly hit the central Great Plains in 2012 (consistent with meteorological studies; see, e.g., Hoerling et al., 2014).

In terms of spring temperature, most of the boreal area experienced lower temperature anomaly while the southern end area (e.g., Texas) experienced abnormal warmer temperature during the 2011 spring. This explains the negative net carbon fluxes during that period, which is also indicated by the vegetation anomaly signals from SIF and EVI. Contrastingly, during the 2012 spring, most temperate area centering at the Great Plains experienced warming (maximum 4–5° above normal), which led to enhancements of vegetation activity. Such enhancements are observed in the northern and southern Great Plains, and the upper Midwest and the southeast. To a certain extent, enhancement due to spring warming and weakening due to summer drought in 2012 occurred at staggered places. The former took place mostly at the forests and crops areas, while the latter located mostly at the grass and crops areas. This intuitively explains the migration effect of

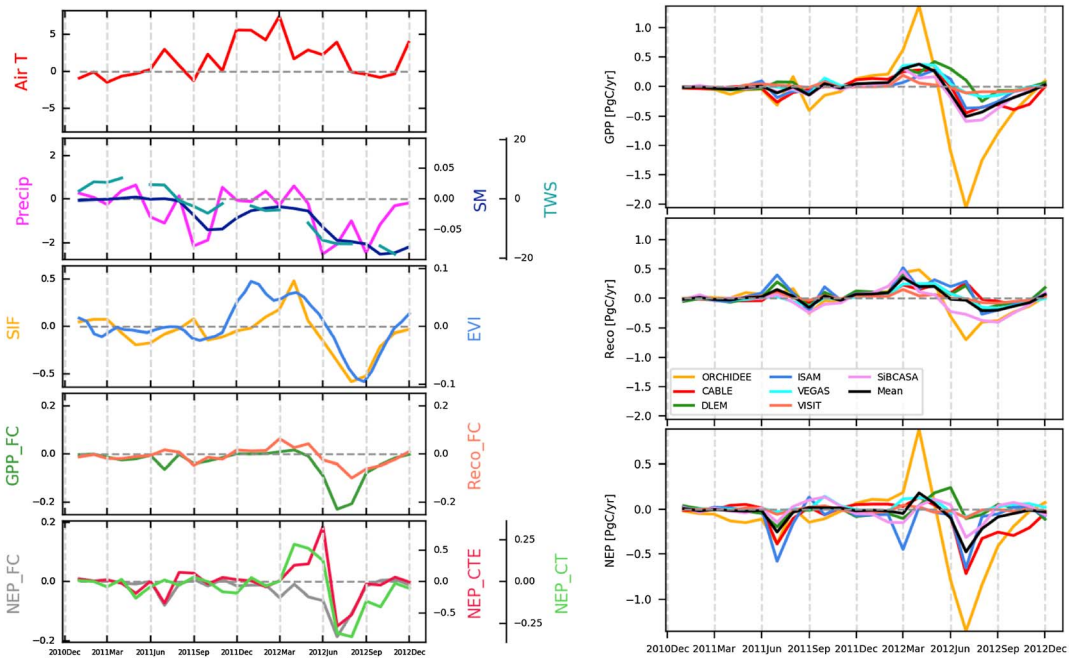

Figure 8. As in Figure 7, but for Region 3 (crops/agriculture).

forests (relatively larger volume on carbon sequestration to crops and grass) to carbon loss resulting from drought impacts at semiarid areas, that is, the Great Plains.

3.2.2. Regional Scale

Considering the geographical distribution of the 2011 and 2012 drought events and ecoregion types, five subregions (as shown in Figure 1) were selected to perform regional-scale analyses of droughts over 2011–2012. Monthly anomalies of air temperature, hydrological and vegetation metrics, and carbon fluxes of three typical regions (grass/shrubs in the southern area, Region 2; crops/agriculture, Region 3; and forests/wooded, Region 4) are shown in Figures 7–9, and two other regions (grass/shrubs in the northern area, Region 1 and tundra/taiga, Region 5) are shown in Figures S4–S5.

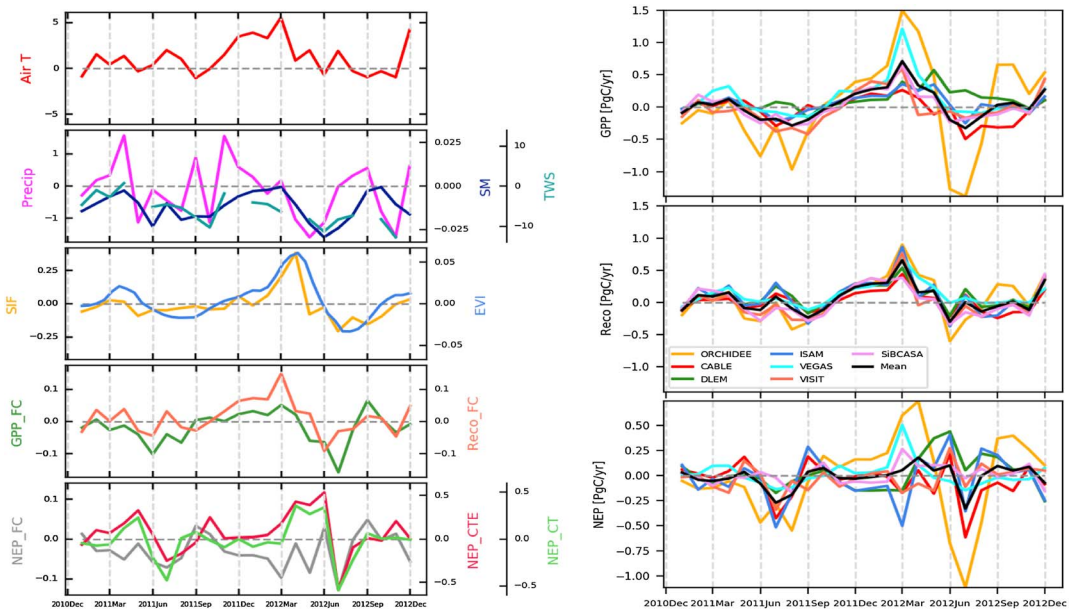

Figure 9. As in Figure 7, but for Region 4 (forests/wooded).

In Region 2, dominated by grass/shrubs in the southern area (Figure 7), NEP declined sharply during the summers of 2011 and 2012 with the former larger in magnitude, which is consistently indicated by the model ensemble and agrees with declines in SIF and EVI. Both GPP and Reco declined, with the former at a larger magnitude, resulting in the negative NEP anomalies in both years. Compared to the grass/shrubs in the northern area as Region 1 (Figure S3), the warmer spring in 2012 brings relatively less NEP enhancement. This slight enhancement has been captured by CTE2016, CT2016, and most DGVMs but not by FLUXCOM. The anomalies of precipitation, SM, and TWS indicate the longtime shortage of water over the whole period in the study region, which contributed to the flux anomalies.

In Region 3, dominated by crops/agriculture (Figure 8), the magnitudes of NEP anomalies in 2012 are larger than those in 2011, as this region was mostly impacted by the 2012 drought. On the whole, the hydrological metrics consistently indicate the summer drought of 2012. Correspondingly, declines of vegetation activity (SIF and EVI) are observed during those periods with concomitant declines in GPP and Reco. In addition, substantial discrepancies in NEP anomalies among these models are observed: CT2016 fails to capture the NEP reduction in 2011 summer, and FLUXCOM fails to capture the NEP enhancement in 2012 spring, while most models consistently capture the NEP reductions in summers of 2011 and 2012 and the enhancement in 2012 spring. Again, a clear increase in NEP during May–June 2012 is detected by DGVMs, CTE2016, and CT2016 but not by FLUXCOM. FLUXCOM fails to capture the enhanced NEP in 2012 spring. Complemented by EO of hydrology and vegetation activity, we found that the 2012 drought caused large decreases of NEP in crops/agriculture, which cannot be compensated by the slight increase of NEP during warming spring.

In Region 4, dominated by forests/wooded (Figure 9), anomalies of GPP and Reco by FLUXCOM and anomalies of NEP by CTE2016 and CT2016 are highly consistent with those from DGVMs and SiBCASA. However, anomalies of NEP in FLUXCOM substantially deviate from those of the other models. On the whole, water scarcities in summers of 2011 and 2012 are consistently indicated by hydrological and vegetation metrics, and the drought impacts are consistently reflected in vegetation metrics and carbon models. A negative NEP anomaly is induced by the drought in 2011, while a near-neutral NEP anomaly is observed as the result of the spring warming and subsequent drought in 2012. Unlike grass/shrubs and crops/agriculture, forests/wooded canceled out the impact of drought through enhancement of carbon uptake during warm spring (Wolf et al., 2016). The two atmospheric inversions support the compensation effect of spring warming to summer drought in the eastern forests/wooded region. Compared to the other regions, the enhancements of GPP and Reco stimulated by spring warming are much larger. It should be noted that large discrepancies of NEP anomalies simulated by different biosphere models are observed.

Among the five subregions, Region 3 (crops/agriculture), Region 2 (grass/shrubs, southern), and Region 1 (grass/shrubs, northern, Figure S4) experienced the largest anomalies of NEP in 2011 and 2012. Although large anomalies of Reco and GPP exist in Region 4 (forests/wooded), the anomaly of NEP is moderate, implying that everything else held equal, the forests/wooded has a better coping capacity in the face of severe droughts, possibly due to access to deeper soil water. In contrast, the crops/agriculture and the southern grass/shrubs show larger NEP reductions associated with droughts.

4. Discussions

4.1. Crucial Role of the Timing and Seasonal Interactions of Climate Extremes in Ecosystem Impacts

This study highlights the crucial role of the timing and seasonal interactions of climate extremes on the terrestrial carbon cycle. Sippel et al. (2016) argued that ecosystem impacts of climate extremes crucially depend on the timing and impacts of climate extremes occurring during different periods of the year can interact and counteract each other. Based on model simulation experiments, Sippel et al. (2017) pointed out that GPP increases in spring compensate GPP reductions in summer in all tested regions in Europe over the past 25 years.

The reaction of summer drought to spring warming occurred because of the tightly coupled process of carbon and water through vegetation stomata (Sippel et al., 2016). Higher spring carbon uptake induced by warming might lead to an earlier depletion of water through increased evapotranspiration, thus exacerbating water limitations in the summer (Sippel et al., 2016; Wolf et al., 2016). In our case, the examples in 2011 and 2012 are contrasting. The 2012 warming spring enhanced summer drought, which brought increased carbon

losses despite increased carbon uptake during spring. Overall, the forests partially mitigated the impacts of drought on crops and grass. However, the year of 2011 experienced an early-spring cold and smaller summer drought at the continental scale. A lasting reduction of net carbon uptake from March to October was consistently simulated by all models, except for AIMs. Compared to 2012 when the net carbon uptake switched from evident increase to reduction, this fluctuation was much milder over the whole year. In order to investigate the effect of spring warming on earlier water depletion, we introduced GLEAM evapotranspiration (ET) v3.1a data set that based on a modified Priestley–Taylor equation (Priestley & Taylor, 1972) for further analysis. This data set has been widely applied in carbon and water cycle studies (Ahlström et al., 2017; Blunden et al., 2017; Forzieri et al., 2017; Miralles et al., 2016; for more details, see the supporting information Text S1). Our result supports that the positive temperature anomaly in 2012 spring enhanced the water depletion through increased evapotranspiration and thus exacerbated the drought condition in summer, but the two were not so strongly coupled in 2011 when the spring temperature was generally below normal (Figures S6–S7). Overall, the interaction between spring warming and summer drought makes a closer to neutral effect on net carbon uptake. Considering the timing and coupling effects of climate extremes would be of great value for understanding the impacts of climate change on the terrestrial carbon cycle.

4.2. Semiarid Ecosystems' Control on the IAV of Regional and Global NEP

Water is a key factor that regulates the IAV of regional and global carbon fluxes (Jung et al., 2017; Seddon et al., 2016). Jung et al. (2017) pointed out that water availability manipulates the IAV of GPP and Reco locally, and to a lesser extent it also holds true for Net ecosystem CO_2 exchange (NEE) at the local scale while temperature plays a dominant role in temporal NEE variations at the global scale. This is also consistent with the conclusion that the semiarid areas control the IAV of terrestrial ecosystems (or NEP) reported by a variety of studies (Ahlström et al., 2015; Fu et al., 2017; Haverd et al., 2016; Marcolla et al., 2017; Poulter et al., 2014; Seddon et al., 2016). Here we show, in line with these studies, that the spatial contributions to changes in NEP are dominated by the semiarid areas of the study domain (see Figure S1). A recent global study based on the FLUXNET data by Schwalm et al. (2010) also reported that agricultural areas show the highest sensitivity of terrestrial carbon sequestration to droughts. Additionally, we also confirmed that forests have an important role in ecosystem service with climate responses different from grasslands, as suggested by Wolf et al. (2016). In contrast with Wolf et al., we found a net carbon loss over North America in 2012 although the warming spring offsets part carbon loss caused by the subsequent summer drought. We note that Wolf et al. (2016) focus on the United States, while we focus on a larger domain, but the anomaly is mostly confined to the U.S. region. The uncertainties from model choice (a single atmospheric inversion data set of NEP used in Wolf et al. (2016)) likely contribute to this discrepancy. It can be found that the two atmospheric inversions estimate clearly larger NEP anomalies in 2012 than the TBMs which our ensemble assessment heavily lies on (see Figure 5). This uncertainty issue will be discussed in section 4.3.

4.3. Uncertainties in Carbon Cycle Models

The uncertainties in carbon fluxes greatly affect the reliabilities of carbon-climate analyses. By combining a comprehensive ensemble of carbon flux products, we have gained more confidence on the analyses of carbon flux variability and drought impacts on carbon fluxes.

We found evident discrepancies in reflecting the seasonal and IAVs among FLUXCOM, TBMs, and AIMs (e.g., Figures 2d and 5a), sometimes disagreeing with those reflected in EO. The in situ flux upscaled product tends to depend on the representativeness of tower sites. Based on our study (e.g., Figures 2 and 5), we highlight that the current FLUXCOM product likely underestimates the IAVs of GPP, Reco, and NEP, and it is also poor at capturing the effects of spring temperature anomalies. Although most TBMs have effectively captured the drought anomalies, a large divergence exists in the estimation of both net and gross carbon fluxes, including magnitudes and phases and thus variabilities and trends, which could bias the analysis of drought impact on the terrestrial carbon cycle. As warned by a previous study, some TBMs have a tendency to overestimate responses to drought (Huang et al., 2016).

AIMs provide a good way to constrain regional and global carbon flux estimates from TBMs with atmospheric CO_2 concentrations. However, the lack of CO_2 observations from in situ or aircrafts limits our ability to robustly constrain the terrestrial carbon flux estimates, especially at finer scales. In this study, AIMs generally captured seasonal anomalies of carbon fluxes in 2011 and 2012, but there are still large discrepancy

on signs and magnitudes at the continental scale; however, they coincided with TBMs well in some regions. Recent developments of estimating CO_2 fluxes from satellite observations open a new window toward improving this situation (Deng et al., 2014; Eldering et al., 2017). In addition, novel approaches that applied atmospheric carbonyl sulfide or SIF to constrain GPP (He et al., 2016; Launois et al., 2015; MacBean et al., 2018; Parazoo et al., 2014) could advance to address process attributions of carbon flux anomalies to climate extremes.

Hence, we need to assimilate more available observations, including in situ flux data, atmospheric CO_2 measurements, and EO of terrestrial ecosystems (Scholze et al., 2017) to constrain carbon flux estimates over large scales. Furthermore, to advance our understanding of the climate evolution processes, developing an explicitly characterized mechanism of droughts in process models is also very demanding.

4.4. Implications of EO to Future Carbon-Climate Studies

Diverse EO relevant to the terrestrial carbon cycle, including vegetation (SIF and EVI) and hydrological conditions (SM and TWS), offered great help in attributing carbon cycle anomalies to climate change. In the context of lacking reliable estimate of carbon fluxes for large scales, the use of EO is extremely important. EO can be viewed as *observations* to complement carbon cycle models. With these satellite-based hydrological and vegetation metrics, we identified if models well represent changes caused by extreme climates. However, we also should notice that these EO metrics used also suffer some uncertainties from retrieving algorithms or sensor performance, which could hamper us in achieving accurate climate change attributions. Hence, developing solid retrieving algorithms and advancing sensor developments are quite important for the global change science community. In the future, synergizing or assimilating EO data into the attribution of the terrestrial carbon cycle anomaly induced by climate extremes is a promising direction.

5. Conclusions

In the present study, we conducted a comprehensive assessment and process attribution of net carbon uptake reductions in North America in 2011 and 2012. Both years were affected by severe summer droughts. In addition, we focused on seasonal components of carbon cycle anomalies, as spring conditions prior to drought differed, with a cold spring in 2011 and an unusually warm spring in 2012. Lastly, we disentangled contributions of different ecoregions to these carbon cycle anomalies. The analyses were based on a comprehensive ensemble of state-of-the-art carbon flux products, meteorological data, and emerging remote sensing metrics.

Our study suggests the strong reductions of net carbon uptake in 2011 and 2012. However, the two years differed in the processes leading up to the anomaly: In 2011, losses are attributed to decreased GPP with increased Reco mainly caused by summer drought, while in 2012 Reco increased stronger than GPP triggered by an extra warmer spring. The warming spring compensated largely the negative carbon anomaly due to the summer drought in 2012. We further identify that crops/agriculture and grass/shrubs in the temperate area contributed the largest proportion of total annual carbon uptake reductions and also dominated the IAVs of net carbon uptake during 2007–2014. Finally, the dominance of these ecoregions in driving carbon cycle anomalies highlights that spring-summer compensatory dynamics can only be seen as an ecoregion-specific phenomenon, rather than operating on continental scales.

Acknowledgments
This research is funded by National Key R&D Program of China (2016YFA0600202). C. Zhang is partially funded by the National Natural Science Foundation of China (grant 41601054). We thank Ivar R. van der Velde for providing the SiBCASA simulations. The CRUNCEP v6 data are available at https://vesg.ipsl.upmc.fr/thredds/catalog/store/p529viov/cruncep/V6_1901_2014/catalog.html. The GLEAM soil moisture and ET data are publicly available at http://www.gleam.eu/. The GRACE TWS data provided by NASA JPL, CSR (University of Texas Center for Space Research), and GFZ (the GeoForschungsZentrum Potsdam) are available at http://podaacftp.jpl.nasa.gov/allData/tellus/L3/land_mass/RL05. The GOME-2 SIF V26 data are publicly available at https://acd-ext.gsfc.nasa.gov/People/Joiner/my_gifs/GOME_F/GOME-F.htm. The MODIS EVI data are available at https://lpdaac.usgs.gov. The TRENDY data (http://dgvm.ceh.ac.uk/) are available from Stephen Sitch (S.A.Sitch@exeter.ac.uk) or Pierre Friedlingstein (p.friedlingstein@exeter.ac.uk) through e-mail request. The FLUXCOM data are publicly available at http://www.fluxcom.org. The CarbonTracker Europe 2016 data are publicly available at http://www.carbontracker.eu. The CarbonTracker 2016 data are publicly available at https://www.esrl.noaa.gov/gmd/ccgg/carbontracker/index.php.

References

Ahlström, A., Canadell, J. G., Schurgers, G., Wu, M., Berry, J. A., Guan, K., & Jackson, R. B. (2017). Hydrologic resilience and Amazon productivity. *Nature Communications*, *8*(1), 387. https://doi.org/10.1038/s41467-017-00306-z

Ahlström, A., Raupach, M. R., Schurgers, G., Smith, B., Arneth, A., Jung, M., et al. (2015). The dominant role of semi-arid ecosystems in the trend and variability of the land CO_2 sink. *Science*, *348*(6237), 895–899. https://doi.org/10.1126/science.aaa1668

Alden, C. B., Miller, J. B., Gatti, L. V., Gloor, M. M., Guan, K., Michalak, A. M., et al. (2016). Regional atmospheric CO_2 inversion reveals seasonal and geographic differences in Amazon net biome exchange. *Global Change Biology*, *22*(10), 3427–3443. https://doi.org/10.1111/gcb.13305

Anav, A., Friedlingstein, P., Kidston, M., Bopp, L., Ciais, P., Cox, P., et al. (2013). Evaluating the land and ocean components of the global carbon cycle in the CMIP5 Earth system models. *Journal of Climate*, *26*(18), 6801–6843. https://doi.org/10.1175/JCLI-D-12-00417.1

Baker, I. T., Prihodko, L., Denning, A. S., Goulden, M., Miller, S., & Da Rocha, H. R. (2008). Seasonal drought stress in the Amazon: Reconciling models and observations. *Journal of Geophysical Research*, *113*, G00B01. https://doi.org/10.1029/2007JG000644

Bastos, A., Janssens, I., Gouveia, C., Trigo, R., Ciais, P., Chevallier, F., et al. (2016). European land CO_2 sink influenced by NAO and East-Atlantic pattern coupling. *Nature Communications*, *7*, 10315. https://doi.org/10.1038/ncomms10315

Biederman, J. A., Scott, R. L., Goulden, M. L., Vargas, R., Litvak, M. E., Kolb, T. E., et al. (2016). Terrestrial carbon balance in a drier world: The effects of water availability in southwestern North America. *Global Change Biology*, *22*(5), 1867–1879. https://doi.org/10.1111/gcb.13222

Blunden, J., Arndt, D. S., Sánchez-Lugo, A., Scambos, T. A., Schreck, C. J. III, Stammerjohn, S., et al. (2017). State of the climate in 2016. *Bulletin of the American Meteorological Society*, *98*, S93–S128.

Cao, Y., Nan, Z., & Cheng, G. (2015). GRACE gravity satellite observations of terrestrial water storage changes for drought characterization in the arid land of northwestern China. *Remote Sensing*, *7*(1), 1021–1047. https://doi.org/10.3390/rs70101021

Ciais, P., Reichstein, M., Viovy, N., Granier, A., Ogée, J., Allard, V., et al. (2005). Europe-wide reduction in primary productivity caused by the heat and drought in 2003. *Nature*, *437*(7058), 529–533. https://doi.org/10.1038/nature03972

Deng, F., Jones, D. B. A., Henze, D. K., Bousserez, N., Bowman, K. W., Fisher, J. B., et al. (2014). Inferring regional sources and sinks of atmospheric CO_2 from GOSAT XCO_2 data. *Atmospheric Chemistry and Physics*, *14*(7), 3703–3727. https://doi.org/10.5194/acp-14-3703-2014

Dorigo, W., Gruber, A., De Jeu, R., Wagner, W., Stacke, T., Loew, A., et al. (2015). Evaluation of the ESA CCI soil moisture product using ground-based observations. *Remote Sensing of Environment*, *162*, 380–395. https://doi.org/10.1016/j.rse.2014.07.023

Dorigo, W., Wagner, W., Albergel, C., Albrecht, F., Balsamo, G., Brocca, L., et al. (2017). ESA CCI soil moisture for improved Earth system understanding: State-of-the art and future directions. *Remote Sensing of Environment*, *203*, 185–215. https://doi.org/10.1016/j.rse.2017.07.001

Doughty, C. E., Metcalfe, D., Girardin, C., Amézquita, F. F., Cabrera, D. G., Huasco, W. H., et al. (2015). Drought impact on forest carbon dynamics and fluxes in Amazonia. *Nature*, *519*(7541), 78–82. https://doi.org/10.1038/nature14213

Eisfelder, C., Klein, I., Niklaus, M., & Kuenzer, C. (2014). Net primary productivity in Kazakhstan, its spatio-temporal patterns and relation to meteorological variables. *Journal of Arid Environments*, *103*(8), 17–30. https://doi.org/10.1016/j.jaridenv.2013.12.005

Eldering, A., Wennberg, P. O., Crisp, D., Schimel, D. S., Gunson, M. R., Chatterjee, A., et al. (2017). The Orbiting Carbon Observatory-2 early science investigations of regional carbon dioxide fluxes. *Science*, *358*(6360), eaam5745. https://doi.org/10.1126/science.aam5745

Forzieri, G., Alkama, R., Miralles, D. G., & Cescatti, A. (2017). Satellites reveal contrasting responses of regional climate to the widespread greening of Earth. *Science*, *356*(6343), 1180–1184. https://doi.org/10.1126/science.aal1727

Friedl, M. A., Sulla-Menashe, D., Tan, B., Schneider, A., Ramankutty, N., Sibley, A., & Huang, X. (2010). MODIS Collection 5 global land cover: Algorithm refinements and characterization of new datasets. *Remote Sensing of Environment*, *114*(1), 168–182. https://doi.org/10.1016/j.rse.2009.08.016

Fu, Z., Dong, J., Zhou, Y., Stoy, P. C., & Niu, S. (2017). Long term trend and interannual variability of land carbon uptake—The attribution and processes. *Environmental Research Letters*, *12*(1). https://doi.org/10.1088/1748-9326/aa5685

Gatti, L., Gloor, M., Miller, J., Doughty, C., Malhi, Y., Domingues, L., et al. (2014). Drought sensitivity of Amazonian carbon balance revealed by atmospheric measurements. *Nature*, *506*(7486), 76–80. https://doi.org/10.1038/nature12957

Gent, P. R., Danabasoglu, G., Donner, L. J., Holland, M. M., Hunke, E. C., Jayne, S. R., et al. (2011). The community climate system model version 4. *Journal of Climate*, *24*(19), 4973–4991. https://doi.org/10.1175/2011JCLI4083.1

Guanter, L., Zhang, Y., Jung, M., Joiner, J., Voigt, M., Berry, J. A., et al. (2014). Global and time-resolved monitoring of crop photosynthesis with chlorophyll fluorescence. *Proceedings of the National Academy of Sciences of the United States of America*, *111*(14), 1327–1333.

Gurney, K. R., Law, R. M., Denning, A. S., Rayner, P. J., Pak, B. C., Baker, D., et al. (2004). Transcom 3 inversion intercomparison: Model mean results for the estimation of seasonal carbon sources and sinks. *Global Biogeochemical Cycles*, *18*, GB1010. https://doi.org/10.1029/2003GB002111

Haverd, V., Smith, B., & Trudinger, C. (2016). Process contributions of Australian ecosystems to interannual variations in the carbon cycle. *Environmental Research Letters*, *11*(5), 054013. https://doi.org/10.1088/1748-9326/11/5/054013

He, W., Ju, W., Chen, H., Peters, W., van der Velde, I., Baker, I., et al. (2016). Constraining gross primary production and ecosystem respiration estimates for North America using atmospheric observations of carbonyl sulfide (OCS) and CO_2. Paper presented at 2016 AGU Fall Meeting Abstracts, San Francisco, CA., U.S.A.

Hoerling, M., Eischeid, J., Kumar, A., Leung, R., Mariotti, A., Mo, K., et al. (2014). Causes and predictability of the 2012 Great Plains drought. *Bulletin of the American Meteorological Society*, *95*(2), 269–282. https://doi.org/10.1175/BAMS-D-13-00055.1

Huang, Y., Gerber, S., Huang, T., & Lichstein, J. W. (2016). Evaluating the drought response of CMIP5 models using global gross primary productivity, leaf area, precipitation and soil moisture data. *Global Biogeochemical Cycles*, *30*, 1827–1846. https://doi.org/10.1002/2016GB005480

Huete, A., Didan, K., Miura, T., Rodriguez, E. P., Gao, X., & Ferreira, L. G. (2002). Overview of the radiometric and biophysical performance of the MODIS vegetation indices. *Remote Sensing of Environment*, *83*(1–2), 195–213. https://doi.org/10.1016/S0034-4257(02)00096-2

Huntzinger, D., Post, W. M., Wei, Y., Michalak, A., West, T. O., Jacobson, A., et al. (2012). North American Carbon Program (NACP) regional interim synthesis: Terrestrial biospheric model intercomparison. *Ecological Modelling*, *232*, 144–157. https://doi.org/10.1016/j.ecolmodel.2012.02.004

Jain, A. K., Meiyappan, P., Song, Y., & House, J. I. (2013). CO_2 emissions from land-use change affected more by nitrogen cycle, than by the choice of land-cover data. *Global Change Biology*, *19*(9), 2893–2906. https://doi.org/10.1111/gcb.12207

Joiner, J., Guanter, L., Lindstrot, R., Voigt, M., Vasilkov, A., Middleton, E., et al. (2013). Global monitoring of terrestrial chlorophyll fluorescence from moderate spectral resolution near-infrared satellite measurements: Methodology, simulations, and application to GOME-2. *Atmospheric Measurement Techniques*, *6*(10), 2803–2823. https://doi.org/10.5194/amt-6-2803-2013

Jönsson, P., & Eklundh, L. (2004). TIMESAT—A program for analyzing time-series of satellite sensor data. *Computers & Geosciences*, *30*(8), 833–845. https://doi.org/10.1016/j.cageo.2004.05.006

Jung, M., Reichstein, M., Schwalm, C. R., Huntingford, C., Sitch, S., Ahlström, A., et al. (2017). Compensatory water effects link yearly global land CO_2 sink changes to temperature. *Nature*, *541*(7638), 516–520. https://doi.org/10.1038/nature20780

Kato, E., Kinoshita, T., Ito, A., Kawamiya, M., & Yamagata, Y. (2013). Evaluation of spatially explicit emission scenario of land-use change and biomass burning using a process-based biogeochemical model. *Journal of Land Use Science*, *8*(1), 104–122. https://doi.org/10.1080/1747423X.2011.628705

Kottek, M., Grieser, J., Beck, C., Rudolf, B., & Rubel, F. (2006). World map of the Köppen-Geiger climate classification updated. *Meteorologische Zeitschrift*, *15*(3), 259–263. https://doi.org/10.1127/0941-2948/2006/0130

Krinner, G., Viovy, N., de Noblet-Ducoudré, N., Ogée, J., Polcher, P., Friedlingstein, P., et al. (2005). A dynamic global vegetation model for studies of the coupled atmosphere-biosphere system. *Global Biogeochemical Cycles*, *19*, GB1015. https://doi.org/10.1029/2003GB002199

Kumar, J., Hoffman, F. M., Hargrove, W. W., & Collier, N. (2016). Understanding the representativeness of FLUXNET for upscaling carbon flux from eddy covariance measurements. *Earth System Science Data Discussions*, 1–25. https://doi.org/10.5194/essd-2016-36

Landerer, F. W., & Swenson, S. (2012). Accuracy of scaled GRACE terrestrial water storage estimates. *Water Resources Research*, *48*, W04531. https://doi.org/10.1029/2011WR011453

Lasslop, G., Reichstein, M., Papale, D., Richardson, A. D., Arneth, A., Barr, A., et al. (2010). Separation of net ecosystem exchange into assimilation and respiration using a light response curve approach: Critical issues and global evaluation. *Global Change Biology*, *16*(1), 187–208. https://doi.org/10.1111/j.1365-2486.2009.02041.x

Launois, T., Peylin, P., Belviso, S., & Poulter, B. (2015). A new model of the global biogeochemical cycle of carbonyl sulfide—Part 2: Use of carbonyl sulfide to constrain gross primary productivity in current vegetation models. *Atmospheric Chemistry and Physics*, *15*(16), 9285–9312. https://doi.org/10.5194/acp-15-9285-2015

Lee, J.-E., Frankenberg, C., van der Tol, C., Berry, J. A., Guanter, L., Boyce, C. K., et al. (2013). Forest productivity and water stress in Amazonia: Observations from GOSAT chlorophyll fluorescence. *Proceedings of the Royal Society B Biological Sciences*, *280*(1761), 20130171. https://doi.org/10.1098/rspb.2013.0171

Le Quéré, C., Andrew, R. M., Canadell, J. G., Sitch, S., Korsbakken, J. I., Peters, G. P., et al. (2016). Global carbon budget 2016. *Earth System Science Data*, *8*(2), 605–649. https://doi.org/10.5194/essd-8-605-2016

Luo, L., Apps, D., Arcand, S., Xu, H., Pan, M., & Hoerling, M. (2017). Contribution of temperature and precipitation anomalies to the California drought during 2012–2015. *Geophysical Research Letters*, *44*, 3184–3192. https://doi.org/10.1002/2016GL072027

MacBean, N., Maignan, F., Bacour, C., Lewis, P., Peylin, P., Guanter, L., et al. (2018). Strong constraint on modelled global carbon uptake using solar-induced chlorophyll fluorescence data. *Scientific Reports*, *8*(1), 1973. https://doi.org/10.1038/s41598-018-20024-w

Marcolla, B., Rödenbeck, C., & Cescatti, A. (2017). Patterns and controls of inter-annual variability in the terrestrial carbon budget. *Biogeosciences*, *14*(16), 3815–3829. https://doi.org/10.5194/bg-14-3815-2017

Martens, B., Gonzalez Miralles, D., Lievens, H., van der Schalie, R., de Jeu, R. A., Fernández-Prieto, D., et al. (2017). GLEAM v3: Satellite-based land evaporation and root-zone soil moisture. *Geoscientific Model Development*, *10*(5), 1903–1925. https://doi.org/10.5194/gmd-10-1903-2017

Miralles, D., Gonzalez, C., Jiménez, M., Jung, D., Michel, A., Ershadi, M., et al. (2016). The WACMOS-ET project—Part 2: Evaluation of global terrestrial evaporation data sets. *Hydrology and Earth System Sciences*, *20*(2), 823–842. https://doi.org/10.5194/hess-20-823-2016

Miralles, D., Gonzalez, T. R. H., Holmes, R. A. M., De Jeu, J. H., Gash, A. G. C. A. M., & Dolman, A. J. (2011). Global land-surface evaporation estimated from satellite-based observations. *Hydrology and Earth System Sciences*, *15*(2), 453–469. https://doi.org/10.5194/hess-15-453-2011

New, M., Hulme, M., & Jones, P. (2000). Representing twentieth-century space–time climate variability. Part II: Development of 1901–96 monthly grids of terrestrial surface climate. *Journal of Climate*, *13*(13), 2217–2238. https://doi.org/10.1175/1520-0442(2000)013%3C2217:RTCSTC%3E2.0.CO;2

Nicolai-Shaw, N., Zscheischler, J., Hirschi, M., Gudmundsson, L., & Seneviratne, S. I. (2017). A drought event composite analysis using satellite remote-sensing based soil moisture. *Remote Sensing of Environment*, *203*, 216–225. https://doi.org/10.1016/j.rse.2017.06.014

Olson, J., Watts, J., & Allison, L. (2000). Major world ecosystem complexes ranked by carbon in live vegetation: A database (NDP-017). Tech. rep., Carbon Dioxide Information Analysis Center, Oak Ridge National Laboratory, Oak Ridge, Tennessee, USA. https://doi.org/10.3334/CDIAC/lue.ndp017

Parazoo, N. C., Bowman, K., Fisher, J. B., Frankenberg, C., Jones, D., Cescatti, A., et al. (2014). Terrestrial gross primary production inferred from satellite fluorescence and vegetation models. *Global Change Biology*, *20*(10), 3103–3121. https://doi.org/10.1111/gcb.12652

Peng, J., Niesel, J., Loew, A., Zhang, S., & Wang, J. (2015). Evaluation of satellite and reanalysis soil moisture products over southwest China using ground-based measurements. *Remote Sensing*, *7*(11), 15,729–15,747. https://doi.org/10.3390/rs71115729

Peters, W., Jacobson, A. R., Sweeney, C., Andrews, A. E., Conway, T. J., Masarie, K., et al. (2007). An atmospheric perspective on North American carbon dioxide exchange: CarbonTracker. *Proceedings of the National Academy of Sciences of the United States of America*, *104*(48), 18,925–18,930. https://doi.org/10.1073/pnas.0708986104

Peters, W., Krol, M., Van Der Werf, G., Houweling, S., Jones, C., Hughes, J., et al. (2010). Seven years of recent European net terrestrial carbon dioxide exchange constrained by atmospheric observations. *Global Change Biology*, *16*(4), 1317–1337. https://doi.org/10.1111/j.1365-2486.2009.02078.x

Peters, W., Miller, J. B., Whitaker, J., Denning, A. S., Hirsch, A., Krol, M. C., et al. (2005). An ensemble data assimilation system to estimate CO_2 surface fluxes from atmospheric trace gas observations. *Journal of Geophysical Research*, *110*, D24304. https://doi.org/10.1029/2005JD006157

Peylin, P., Law, R., Gurney, K., Chevallier, F., Jacobson, A., Maki, T., et al. (2013). Global atmospheric carbon budget: Results from an ensemble of atmospheric CO_2 inversions. *Biogeosciences*, *10*(10), 6699–6720. https://doi.org/10.5194/bg-10-6699-2013

Piao, S., Sitch, S., Ciais, P., Friedlingstein, P., Peylin, P., Wang, X., et al. (2013). Evaluation of terrestrial carbon cycle models for their response to climate variability and to CO_2 trends. *Global Change Biology*, *19*(7), 2117–2132. https://doi.org/10.1111/gcb.12187

Potter, C. S., Randerson, J. T., Field, C. B., Matson, P. A., Vitousek, P. M., Mooney, H. A., & Klooster, S. A. (1993). Terrestrial ecosystem production: A process model based on global satellite and surface data. *Global Biogeochemical Cycles*, *7*, 811–841. https://doi.org/10.1029/93GB02725

Poulter, B., Frank, D., Ciais, P., Myneni, R. B., Andela, N., Bi, J., et al. (2014). Contribution of semi-arid ecosystems to interannual variability of the global carbon cycle. *Nature*, *509*(7502), 600–603. https://doi.org/10.1038/nature13376

Priestley, C., & Taylor, R. (1972). On the assessment of surface heat flux and evaporation using large-scale parameters. *Monthly Weather Review*, *100*(2), 81–92. https://doi.org/10.1175/1520-0493(1972)100%3C0081:OTAOSH%3E2.3.CO;2

Reichstein, M., Falge, E., Baldocchi, D., Papale, D., Aubinet, M., Berbigier, P., et al. (2005). On the separation of net ecosystem exchange into assimilation and ecosystem respiration: Review and improved algorithm. *Global Change Biology*, *11*(9), 1424–1439. https://doi.org/10.1111/j.1365-2486.2005.001002.x

Restrepo-Coupe, N., Levine, N. M., Christoffersen, B. O., Albert, L. P., Wu, J., Costa, M. H., et al. (2017). Do dynamic global vegetation models capture the seasonality of carbon fluxes in the Amazon basin? A data-model intercomparison. *Global Change Biology*, *23*(1), 191–208. https://doi.org/10.1111/gcb.13442

Rubel, F., Brugger, K., Haslinger, K., & Auer, I. (2017). The climate of the European Alps: Shift of very high resolution Köppen-Geiger climate zones 1800–2100. *Meteorologische Zeitschrift*, *26*(2), 115–125. https://doi.org/10.1127/metz/2016/0816

Schaefer, K., Collatz, G. J., Tans, P., Denning, A. S., Baker, I., Berry, J., et al. (2008). Combined simple biosphere/Carnegie-Ames-Stanford approach terrestrial carbon cycle model. *Journal of Geophysical Research*, *113*, G03034. https://doi.org/10.1029/2007JG000603

Scholze, M., Buchwitz, M., Dorigo, W., Guanter, L., & Quegan, S. (2017). Reviews and syntheses: Systematic Earth observations for use in terrestrial carbon cycle data assimilation systems. *Biogeosciences*, *14*(14), 3401–3429. https://doi.org/10.5194/bg-14-3401-2017

Schwalm, C. R., Williams, C. A., Schaefer, K., Arneth, A., Bonal, D., Buchmann, N., et al. (2010). Assimilation exceeds respiration sensitivity to drought: A FLUXNET synthesis. *Global Change Biology*, *16*(2), 657–670. https://doi.org/10.1111/j.1365-2486.2009.01991.x

Schwalm, C. R., Williams, C. A., Schaefer, K., Baldocchi, D., Black, T. A., Goldstein, A. H., et al. (2012). Reduction in carbon uptake during turn of the century drought in western North America. *Nature Geoscience*, *5*(8), 551–556. https://doi.org/10.1038/ngeo1529

Schwalm, C. R., Wrl, A., Michalak, A. M., Fisher, J. B., Biondi, F., Koch, G., et al. (2017). Global patterns of drought recovery. *Nature*, *548*(7666), 202–205. https://doi.org/10.1038/nature23021

Scott, R. L., Biederman, J. A., Hamerlynck, E. P., & Barron-Gafford, G. A. (2015). The carbon balance pivot point of southwestern US semiarid ecosystems: Insights from the 21st century drought. *Journal of Geophysical Research: Biogeosciences*, *120*, 2612–2624. https://doi.org/10.1002/2015JG003181

Seddon, A. W., Macias-Fauria, M., Long, P. R., Benz, D., & Willis, K. J. (2016). Sensitivity of global terrestrial ecosystems to climate variability. *Nature*, *531*(7593), 229–232. https://doi.org/10.1038/nature16986

Sellers, P., Randall, D., Collatz, G., Berry, J., Field, C., Dazlich, D., et al. (1996). A revised land surface parameterization (SiB2) for atmospheric GCMs. Part I: Model formulation. *Journal of Climate*, *9*(4), 676–705. https://doi.org/10.1175/1520-0442(1996)009%3C0676:ARLSPF%3E2.0.CO;2

Sippel, S., Forkel, M., Rammig, A., Thonicke, K., Flach, M., Martin, H., et al. (2017). Contrasting and interacting changes in simulated spring and summer carbon cycle extremes in European ecosystems. *Environmental Research Letters*, *12*(7), 075006. https://doi.org/10.1088/1748-9326/aa7398

Sippel, S., Zscheischler, J., & Reichstein, M. (2016). Ecosystem impacts of climate extremes crucially depend on the timing. *Proceedings of the National Academy of Sciences of the United States of America*, *113*(21), 5768–5770. https://doi.org/10.1073/pnas.1605667113

Sitch, S., Friedlingstein, P., Gruber, N., Jones, S., Murray-Tortarolo, G., Ahlström, A., et al. (2015). Recent trends and drivers of regional sources and sinks of carbon dioxide. *Biogeosciences*, *12*(3), 653–679. https://doi.org/10.5194/bg-12-653-2015

Sun, Y., Fu, R., Dickinson, R., Joiner, J., Frankenberg, C., Gu, L., et al. (2015). Drought onset mechanisms revealed by satellite solar-induced chlorophyll fluorescence: Insights from two contrasting extreme events. *Journal of Geophysical Research: Biogeosciences*, *120*, 2427–2440. https://doi.org/10.1002/2015JG003150

Swenson, S., & Wahr, J. (2006). Post-processing removal of correlated errors in GRACE data. *Geophysical Research Letters*, *33*, L08402. https://doi.org/10.1029/2005GL025285

Thompson, R. L., Patra, P., Chevallier, F., Maksyutov, S., Law, R., Ziehn, T., et al. (2016). Top-down assessment of the Asian carbon budget since the mid 1990s. *Nature Communications*, *7*, 10724. https://doi.org/10.1038/ncomms10724

Tian, H., Chen, G., Lu, C., Xu, X., Hayes, D. J., Ren, W., et al. (2015). North American terrestrial CO_2 uptake largely offset by CH_4 and N_2O emissions: Toward a full accounting of the greenhouse gas budget. *Climatic Change*, *129*(3–4), 413–426. https://doi.org/10.1007/s10584-014-1072-9

Tramontana, G., Jung, M., Schwalm, C. R., Ichii, K., Camps-Valls, G., Ráduly, B., et al. (2016). Predicting carbon dioxide and energy fluxes across global FLUXNET sites with regression algorithms. *Biogeosciences*, *13*(14), 4291–4313. https://doi.org/10.5194/bg-13-4291-2016

van der Laan-Luijkx, I. T., van der Velde, I. R., van der Veen, E., Tsuruta, A., Stanislawska, K., Babenhauserheide, A., et al. (2017). The CarbonTracker Data Assimilation Shell (CTDAS) v1. 0: Implementation and global carbon balance 2001–2015. *Geoscience Model Development*, *10*(7), 2785–2800. https://doi.org/10.5194/gmd-10-2785-2017

van der Molen, M. K., Dolman, A. J., Ciais, P., Eglin, T., Gobron, N., Law, B. E., et al. (2011). Drought and ecosystem carbon cycling. *Agricultural and Forest Meteorology*, *151*(7), 765–773. https://doi.org/10.1016/j.agrformet.2011.01.018

van der Velde, I., Miller, J., Schaefer, K., van der Werf, G., Krol, M., & Peters, W. (2014). Terrestrial cycling of $^{13}CO_2$ by photosynthesis, respiration, and biomass burning in SiBCASA. *Biogeosciences*, *11*(23), 6553–6571. https://doi.org/10.5194/bg-11-6553-2014

Velpuri, N. M., Senay, G. B., & Morisette, J. T. (2016). Evaluating new SMAP soil moisture for drought monitoring in the rangelands of the US High Plains. *Rangelands*, *38*(4), 183–190. https://doi.org/10.1016/j.rala.2016.06.002

von Buttlar, J., Zscheischler, J., Rammig, A., Sippel, S., Reichstein, M., Knohl, A., et al. (2018). Impacts of droughts and extreme temperature events on gross primary production and ecosystem respiration: A systematic assessment across ecosystems and climate zones. *Biogeosciences*, *15*(5), 1293–1318. https://doi.org/10.5194/bg-15-1293-2018

Wang, S., Huang, C., Zhang, L., Lin, Y., Cen, Y., & Wu, T. (2016). Monitoring and assessing the 2012 drought in the Great Plains: Analyzing satellite-retrieved solar-induced chlorophyll fluorescence, drought indices, and gross primary production. *Remote Sensing*, *8*(2), 61. https://doi.org/10.3390/rs8020061

Wang, Y., Law, R., & Pak, B. (2010). A global model of carbon, nitrogen and phosphorus cycles for the terrestrial biosphere. *Biogeosciences*, *7*(7), 2261–2282. https://doi.org/10.5194/bg-7-2261-2010

Wei, Y., Liu, S., Huntzinger, D. N., Michalak, A. M., Viovy, N., Post, W. M., et al. (2014). The North American Carbon Program Multi-scale Synthesis and Terrestrial Model Intercomparison Project—Part 2: Environmental driver data. *Geoscientific Model Development*, *7*(6), 2875–2893. https://doi.org/10.5194/gmd-7-2875-2014

Wolf, S., Eugster, W., Ammann, C., Häni, M., Zielis, S., Hiller, R., et al. (2013). Contrasting response of grassland versus forest carbon and water fluxes to spring drought in Switzerland. *Environmental Research Letters*, *8*(3), 035007. https://doi.org/10.1088/1748-9326/8/3/035007

Wolf, S., Keenan, T. F., Fisher, J. B., Baldocchi, D. D., Desai, A. R., Richardson, A. D., et al. (2016). Warm spring reduced carbon cycle impact of the 2012 US summer drought. *Proceedings of the National Academy of Sciences*, *113*(21), 5880–5885.

Xie, Z., Huete, A., Restrepo-Coupe, N., Ma, X., Devadas, R., & Caprarelli, G. (2016). Spatial partitioning and temporal evolution of Australia's total water storage under extreme hydroclimatic impacts. *Remote Sensing of Environment*, *183*, 43–52. https://doi.org/10.1016/j.rse.2016.05.017

Yang, Y., Long, D., Guan, H., Scanlon, B. R., Simmons, C. T., Jiang, L., & Xu, X. (2014). GRACE satellite observed hydrological controls on interannual and seasonal variability in surface greenness over mainland Australia. *Journal of Geophysical Research: Biogeosciences*, *119*, 2245–2260. https://doi.org/10.1002/2014JG002670

Yi, H., & Wen, L. (2016). Satellite gravity measurement monitoring terrestrial water storage change and drought in the continental United States. *Scientific Reports*, *6*(1), 19909. https://doi.org/10.1038/srep19909

Zeng, N., Mariotti, A., & Wetzel, P. (2005). Terrestrial mechanisms of interannual CO_2 variability. *Global Biogeochemical Cycles*, *19*, GB1016. https://doi.org/10.1029/2004GB002273

Zhang, Y., Guanter, L., Berry, J. A., Tol, C. V. D., Yang, X., Tang, J., & Zhang, F. (2016). Model-based analysis of the relationship between sun-induced chlorophyll fluorescence and gross primary production for remote sensing applications. *Remote Sensing of Environment*, *187*, 145–155. https://doi.org/10.1016/j.rse.2016.10.016

Zhao, M., & Running, S. W. (2010). Drought-induced reduction in global terrestrial net primary production from 2000 through 2009. *Science*, *329*(5994), 940–943. https://doi.org/10.1126/science.1192666

Zscheischler, J., Mahecha, M. D., Von Buttlar, J., Harmeling, S., Jung, M., Rammig, A., et al. (2014). A few extreme events dominate global interannual variability in gross primary production. *Environmental Research Letters*, *9*(3), 035001. https://doi.org/10.1088/1748-9326/9/3/035001